scientific reports

Check for updates

OPEN

Spatial and temporal variation in surface nitrate and phosphate in the Northern Gulf of Mexico over 35 years

Kailani G. Acosta[1✉], Andrew R. Juhl[1], Ajit Subramaniam[1] & Solange Duhamel[2]

Dissolved inorganic nutrient concentrations in the surface waters (0 to 5 m) of the Northern Gulf of Mexico (NGoM) were analyzed from 1985 to 2019 (> 10,000 observations) to determine spatiotemporal trends and their connection to nutrients supplied from the Mississippi/Atchafalaya River (MAR). In the NGoM, annual mean dissolved inorganic P (DIP) concentrations increased significantly over time, while dissolved inorganic N (DIN) concentrations showed no temporal trend. With greater salinity, mean DIN:DIP decreased from above the Redfield ratio of 16 to below it, reflecting DIN losses and the more conservative behavior of DIP with salinity. Over the same time period, annual mean P (total dissolved P, DIP, dissolved organic P) loading from the MAR to the NGoM significantly increased, annual mean DIN and total dissolved N loading showed no temporal trend, and dissolved organic N loading significantly decreased. Though DIP increased in the MAR, MAR DIP alone was insufficient to explain the surface distribution of DIP with salinity. Therefore, increases in surface DIP in the NGoM are not simply a reflection of increasing MAR DIP, pointing to temporal changes in other DIP sources. The increase in NGoM DIP suggests greater N limitation for phytoplankton, with implications for N fixation and nutrient management.

Marine primary production is often mediated and limited by the bioavailability of dissolved nutrients such as nitrogen (N) and phosphorus (P)[1–3]. Studies have shown that N limitation of marine primary production is more widespread than P limitation[3,4], though P availability may play an important role over long time scales[5,6], and in certain locations, such as the Northern Gulf of Mexico[7]. Surface ocean N and P concentrations are spatially and temporally variable as a result of many complex processes such as uptake by phytoplankton and bacteria, including luxury consumption[8], N fixation[9], N loss through denitrification in low oxygen regions[10], biological and chemical conversion of inorganic and organic N and P[11,12], legacy nutrients stored in the landscape[13,14], and external anthropogenic inputs[15,16]. These processes can lead to deviations in organic matter production and dissolved nutrient ratios from the canonical 106C:16N:1P of Redfield proportions[3,12,17]. For example, rivers, estuaries, and coastal regions typically have higher dissolved inorganic N and P (DIN and DIP) concentrations and DIN:DIP than offshore regions[18], where average surface DIN:DIP is about 13[5]. Meanwhile, in the majority (~ 78%) of the world's large rivers, DIN:DIP exceeds 16, and increases with DIN concentrations[19]. These spatial patterns could be explained by net relative losses of DIN[5,20], and/or by a relative net gain of DIP from bioconversion of dissolved organic P (DOP) to DIP as salinity increases from nearshore to offshore waters[21,22].

In this study, we focus on the spatial and temporal variability of surface DIN and DIP concentrations over the last 35 years in the Northern Gulf of Mexico (NGoM) along the salinity gradient from the Mississippi and Atchafalaya Rivers (MAR) to offshore oceanic waters. Annual mean MAR discharge is more than 15 times that of all other rivers that drain into the NGoM[23], thus we focus on annual mean MAR discharge as the main source of nutrients and freshwater into the NGoM system. The size, direction, and location of the NGoM freshwater plume change in concert with varying volume and timing of river discharge as well as wind speed and direction, therefore further influencing nutrient and salinity patterns[24–26]. Riverine freshwater plumes generally extend westward in the NGoM through the Louisiana Coastal Current, though wind forcing pushes buoyant plumes eastward depending on the time of year[23,27]. Physical drivers such as onshore winds and salinity cause MAR plume waters and its nutrients, sediments, and organic matter to be transported westward alongshore and

[1]Lamont-Doherty Earth Observatory, Columbia University, 61 Route 9W, Palisades, NY 10964, USA. [2]Department of Molecular and Cellular Biology, University of Arizona, Tucson, AZ 85721, USA. ✉email: kailani.acosta@columbia.edu

eastward along the approximately 200 m depth shelf break[27,28]. The majority of riverine N and P are retained in nearshore regions of the NGoM in the fall and winter[29], and spread offshore in the summer, though N typically declines more dramatically as a function of salinity than P[30,31]. When averaged annually, the majority of surface water DIN (70%) is retained on the shelf, while 30% of DIN is transported further offshore[32]. Together the MAR are the main sources of freshwater and nutrients into the NGoM, on average delivering 80% of the freshwater, 91% of the N loading, and 88% of the P loading into the system with a combined mean flow of approximately 21,500 m^3 s^{-1}[33–35].

Over the last 200 years, many aspects of the MAR watershed have been altered by changing water demands, fluctuating sediment yields, navigational amendments, and flood-control systems[36]. The MAR's water quality and chemistry has been substantially impacted by changes in land use, agriculture, industry, and sewage effluent[37,38]. From the 1950s to 1990s, TDN loading (primarily driven by increasing DIN loading) from the MAR to the NGoM tripled, and TDP loading doubled[35,36]. Since then, TDN loading has not appreciably increased, and has even stabilized in some locations[35,39]. Earlier studies found no temporal trends in DIP or TDP from the 1970s to 1990s[40]. Temporal trends in MAR nutrient loading are similar to global trends in the latter part of the twentieth century, though MAR N fluxes increased more, and P fluxes increased less, than the global average[41].

Despite the increase in N loading from the MAR, empirical studies indicate a predominance of N limitation of phytoplankton in the NGoM[11], and isotopic evidence indicates that the majority of N incorporated into planktonic biomass in the NGoM originates from MAR loading[35]. Nevertheless, observations of P limitation have been reported, especially at intermediate salinities within the MAR plume during spring and summer[42–44]. Multiple studies have investigated the connections between MAR flow and NGoM nutrient concentrations[31,45–47]. Lohrenz et al. (1999) found a positive correlation between MAR river discharge and MAR N:P, and in their 1990 study concluded that riverine nutrient supply constraints were a controlling factor of biomass and production at high salinities. Wysocki et al. (2006) further established that the spatial distribution of NGoM nutrients changed with MAR flow, with higher NGoM nutrient concentrations observed further offshore during periods of higher discharge. However, Cardona et al. (2016) concluded that MAR discharge alone was insufficient to predict NGoM surface nutrient concentrations, given low nutrient concentrations observed following high flow periods.

Additionally, MAR discharge and nutrient flux are tied to the spatial and temporal variability of the summer hypoxic area, or "dead zone" in the NGoM (characterized by dissolved oxygen content of < 2 mg L^{-1})[48]. The increase in MAR DIN loading from the 1950s to 1990s coincided with increased NGoM primary production, sediment C accumulation, and hypoxia—hypoxia did not appear as widespread or recurrent prior to the 1950s increase in DIN[35,49,50]. The areal extent of the NGoM dead zone is also correlated with MAR DIN loading and with primary production only in the MAR plume, not the full shelf area of the GoM[35,44,51]. Over time, the relationship between DIN loading and hypoxic area has changed, with the same amount of DIN loading in recent years leading to larger hypoxic areas than prior to the early 1990s[52,53]. Despite the importance of DIN in NGoM hypoxia, model simulations show that P limitation may play an important role by shifting primary production downstream within the plume and decreasing the area of hypoxic bottom water, due to changes in where primary production occurs and whether respiration occurs in the sediment or water column[54]. Field studies are consistent with model findings, as P limitation of phytoplankton delays the assimilation of riverine DIN in the summer and drives primary production over a larger region beyond shelf plume waters[44].

The purpose of this study was to understand the patterns of DIN, DIP, and DIN:DIP on multiple scales in the NGoM; temporally (1985 to 2019) and spatially (shelf to offshore) in surface waters (0 to 5 m). This study represents an expanded view of nutrient trends and spatial patterns in the NGoM in the context of ongoing efforts to manage MAR nutrient loads to the NGoM, especially for N[55]. Many other studies have characterized the surface nutrient trends in the NGoM, though more have focused on more limited areas or timespans[31,36,56]. Based on our temporal and spatial nutrient analyses, we address the following objectives: (a) to delineate spatiotemporal trends in surface nutrient (DIN and DIP) concentrations and in the resulting DIN:DIP in the MAR and NGoM from 1985 to 2019; (b) to evaluate MAR nutrients as potential drivers of NGoM nutrient change over time and space; and (c) to determine whether nutrient shifts described in previous studies have persisted (i.e., changes in nutrient regime, anthropogenic impacts). These objectives aim to examine how changes in nutrient delivery through the MAR contribute to variations in surface nutrients in the NGoM over time and space.

Methodology

Data description

The NGoM nutrient data set was compiled following methods used in Cardona et al. (2016), and enhanced by including a larger salinity range (i.e., including salinities lower than 11 ppt), adding additional nutrient samples post-2012, and other pre-2012 observations that had not been included in the earlier study. Our study's data set included only surface (0 to 5 m collection depth) nutrient data in the NGoM (defined as coordinates − 98°, − 79° to 22.5°, 31°; Fig. 1) from 1985 to 2019, with most data collected in the summer months (Fig. S2). NGoM surface data were used to ensure that samples were influenced by the MAR plume. Numerous studies of nutrients, phytoplankton, and riverine transport have entirely or primarily focused on the upper few meters of the NGoM water column (e.g., Cardona et al., 2016, Wysocki et al., 2006). Thus, the results of this study elaborate on the context provided by earlier work.

The criteria for the compiled NGoM surface nutrient data included: 0 to 5 m sampling depth, collection date from 1985 to 2019, and study location in the northern portion of the GoM (within coordinate box listed above). Data also needed to include salinity (0–37 ppt), and surface DIN and DIP concentrations in μM, if data were not listed in μmoles/L or μM, they were converted to μM. For quality assurance, data with salinities greater than 37 ppt or without corresponding salinity values were excluded (i.e., this excluded all data points from cruises from 1988 and 2014). In addition, 39 NGoM datapoints (from n = 10,007 total) with nutrient values above 8 μM

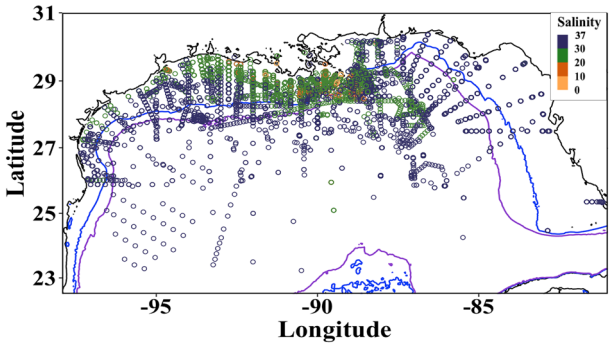

Figure 1. NGoM nutrient sampling locations 1985–2019. Circles represent individual surface samples (0–5 m collection depth). Circle color denotes sample salinity. Bathymetry isobaths denote the 60 m (blue line) and 200 m (purple line) depth isobaths, respectively.

DIP or 110 µM DIN were excluded as they were greater than three standard deviations above the mean. The bottom depth for each sample coordinate was calculated with the *marmap* R package for all data within coordinates − 98°, − 79°, and 20°, 31°[57]. These data were compiled from a variety of sources with varied collection and analysis data validation methods; with this in mind, we verified the data in comparison to data from other years and regions, covering a large portion of the surface waters of the NGoM over 35 years. Data with these criteria were compiled from the Biological & Chemical Oceanography Data Management Office (BCO-DMO), National Oceanic and Atmospheric Administration National Centers for Environmental Information—World Ocean Database (NOAA NCEI WOD), United States Geological Survey (USGS), and Gulf of Mexico Research Initiative Information and Data Cooperative (GRIIDC) (Table S1).

Uptake rates of NH_4^+ in the MAR plume can be comparable to those for NO_3^-; however, we operationally defined DIN as the $NO_2^- + NO_3^-$ concentration, excluding NH_4^+ because it was relatively rarely measured in the MAR and NGoM databases and was often near or below the detection limit or a minor fraction of DIN when it was quantified. Typically, NH_4^+ is rapidly transformed into $NO_2^- + NO_3^-$, with concentrations from 0.17 to 0.44 µM and little spatial variability in both the lower MAR and NGoM[58,59]. Prior studies of this region similarly focused on $NO_2^- + NO_3^-$. USGS historical records for the Mississippi River at St. Francisville, LA, that we used in our MAR nutrient comparison[31,60,61], also define inorganic N as $NO_2^- + NO_3^-$. The majority of surveyed studies did not measure organic forms of N and P, so analyses were conducted only using inorganic nutrient data.

For some analyses, the surface nutrient data were subset into three different spatial regions: hypoxic region (data within − 88° to − 95° and 27° to 29° with bottom depths of < 60 m, Figure S3a), shelf region (data with bottom depths of < 200 m, Fig. S3b), and offshore region (data with bottom depths of > 200 m, Fig. S3c). The hypoxic region defined here was a shallow subset of the shelf region where hypoxic bottom waters are most likely to be found; the boundaries of the hypoxic region did not change through time in these analyses, though the actual area measured with hypoxic bottom water varies seasonally and annually[35].

MAR data (nutrient loading, nutrient concentrations, discharge, and suspended sediment concentrations) were also compiled for 1985 to 2019 from the St. Francisville, Louisiana USGS National Water Quality Network (NWQN) program monitoring station because it had the longest running nutrient data (dissolved nutrients measured multiple times per year since 1954) in the lower portion of the MAR, and it is located close to the point where the Atchafalaya River diverges from the Mississippi, covering a drainage area greater than 2.9×10^6 km^2[62]. Many other NGoM studies similarly use MAR nutrient data from the St. Francisville, LA USGS monitoring station[36,63,64]. In addition to DIN ($NO_2^- + NO_3^-$ as N, filtered, mg L^{-1}) and DIP (orthophosphate, filtered, mg L^{-1}), the USGS MAR water quality data included TDN ($NO_2^- + NO_3^- + NH_4^+$ + organic-N, filtered, mg L^{-1}), TDP (filtered, mg L^{-1}), dissolved organic N (DON; filtered, mg L^{-1}), and dissolved organic P (DOP; filtered, mg L^{-1}), that were not included within the NGoM nutrient data set because they were rarely measured compared to DIN and DIP in the NGoM. MAR data were compiled for nutrients (in mg L^{-1}), discharge (in tons, then converted to kg year^{-1}), loading (in tons, then converted to kg year^{-1}) and suspended sediments from all available dates between 1985 and 2019.

The MAR basin has been a location of intense streamflow and large-scale water quality monitoring for decades; this study tests whether the MAR nutrient fluxes can explain spatial and temporal nutrient trends in the NGoM as a whole. MAR St. Francisville water quality loads are sourced from USGS (USGS Station 07373420) as indicated in Lee (2022). USGS computed annual, flow-normalized water-quality loads (mean annual sample n = 16) using the USGS Load Estimator (LOADEST) program and Weighted Regressions on Time, Discharge, and Season method (WRTDS) between 1985 and 2019 using available discrete water-quality and streamflow information[61]. Nutrient fluxes were calculated using Adjusted Maximum Likelihood Estimation (AMLE) using the LOADEST program to compute nutrient loads using a 10-year moving window approach in the MAR basin[61,65]. Load estimation methods included the log of cubic streamflow, time (annual, seasonal, monthly), and historical streamflow conditions[61]. The WRTDS water quality data for the MAR is used by the Mississippi River/Gulf of Mexico Hypoxia Task Force to meet their goals of reducing the hypoxic zone in the GoM to a 5 year moving average of 5000 km^2[61,65]. To determine the annual amount of MAR discharge at St. Francisville, annual flow for a given water year was converted from daily cubic meters second^{-1} to acre-feet day^{-1} then averaged annually.

For WRTDS loads calculated for the MAR at St, Francisville, WRTDS calibration records existed from 1980 to 2019 for loads of TDN, TDP, DIN, and suspended sediment concentrations, while DIP loads were analyzed and calibrated from 1982 to 2019[61,65]. These WRTDS loads are assumed to be the most accurate load estimates for any given year[65]. In our study, the MAR annual WRTDS nutrient load data was compared to MAR nutrient data using comparable analyses to determine correlations and compare trends in nutrient concentrations over time and space.

Data analyses

All statistical analyses used a significance level of 0.05. NGoM temporal nutrient trends were evaluated by linear regressions of annual mean DIN and DIP concentrations and DIN:DIP against time. Similarly, temporal trends in MAR data were assessed using linear regressions of annual means for each parameter over time (nutrient loading, nutrient concentrations, discharge, suspended sediment). Temporal regression analyses in this study set 1985 as year zero so that the regression equations provided meaningful y-intercepts. Oftentimes, long successive time-series contain autocorrelation of data[66]. To remove potential autocorrelation in the time series data, we based the analysis on annual mean NGoM and MAR nutrient concentrations, and also tested for autocorrelation using Durbin-Watson tests. For data with significant autocorrelation, Cochrane-Orcutt transformation was used, and Durbin-Watson tests were run again to confirm reduction of autocorrelation below significance. The Cochrane-Orcutt estimation and subsequent transformation also accounted for heteroscedasticity in the data, confirmed by Breusch-Pagan tests. In addition to linear regression, changepoint analyses of mean annual nutrient concentrations were conducted using a regression model in R package *changepoint* with segmented relationships for annual mean DIN and DIP over time to determine whether monotonic analyses were appropriate for the nutrient time series. Changepoint analyses identify statistically significant changes or breaks in trends over time. After standardizing year and nutrient concentration (DIN, DIP) variables, we then used a Markov Chain Monte Carlo simulation to fit a Bayesian changepoint model. The changepoint in the data represents a gap or change in the distribution of the nutrient data in a given year. If there are no significant changepoints, then monotonic analyses are best suited for the data.

Pearson correlation analyses tested for significant temporal relationships between annual mean MAR discharge, nutrient concentrations, and nutrient loading with the corresponding annual mean NGoM nutrient concentrations. Parallel analyses focused on each of the three regional data subsets: hypoxic, shelf, and offshore regions. Pearson correlation analyses also compared annual mean nutrient concentrations in the shelf and offshore regions to each other. Finally, Pearson correlation analyses compared the annual area of hypoxic bottom water[35] to mean annual MAR nutrient loading and mean annual NGoM nutrient concentrations as a whole, as well as in each spatial region.

Next, the NGoM nutrient data set was analyzed in relation to sample salinity to incorporate dilution along the continuum from the MAR endmember to the oceanic endmember into the analyses of nutrient concentrations. While there was generally a trend of increasing salinity going offshore, it should be noted that nearly the full range of salinities was found in both shelf and offshore regions, and salinity plots were thus not strictly analogous to geographic patterns (i.e., some samples found beyond the 200 m isobath had salinities less than 20; Fig. S2). Low salinity offshore waters were located within the freshwater plume, which varies over time and space with environmental variables such as river discharge, wind speed, and direction[67]. Nutrient data were regressed against salinity using a variety of functions, including linear, exponential, and power functions; within monotonic functions, bivariate linear regression of ln-transformed data provided the highest r^2 values and significance. To account for zero values in the data set prior to the ln-transformation, we added a reasonable detection limit to all samples (0.05 μM for DIN, 0.03 μM for DIP), similar to that used in Cardona et al. (2016). Linear regressions of ln[DIN], ln[DIP], and ln(DIN:DIP) vs. salinity described the general trends of decreasing nutrient concentrations along the salinity gradient due to dilution and loss (e.g., phytoplankton uptake). To improve visualization, especially of low nutrient concentrations, figures show untransformed data plotted with log-scale y-axes. These regressions and their presentation on plots were primarily intended to show general trends of nutrient concentrations with salinity.

Nutrient data were also compared to conservative mixing functions, calculated by linearly connecting the long-term mean MAR TDN, TDP, DIN, and DIP concentrations at St. Francisville, LA at 0 ppt salinity to the minimum ocean endmember nutrient concentration (the detection limits mentioned above) at 37 ppt (Fig. S1). This line described the expected decline of nutrient concentration due to dilution of MAR water with the offshore endmember. Note that on the semi-log plots shown in later figures, the mixing functions appear curved. To understand how the relationship between nutrient concentrations and salinity changed through time relative to the conservative mixing function, we calculated the residuals of each data point compared to the respective conservative mixing function along the salinity gradient. Negative residuals signified loss of nutrients relative to the MAR endmember that exceeded the decline expected due to mixing with the offshore endmember (e.g., due to phytoplankton uptake). Positive residuals indicated excess inorganic nutrients relative to the two-endmember function, suggesting a source in addition to the MAR endmember. Analogous residual analyses were also conducted on the hypoxic, shelf, and offshore regional subsets.

Results

Spatiotemporal changes in annual mean NGoM DIN, DIP, and DIN:DIP

NGoM DIN concentrations (1985–2019) were highly variable and showed no significant temporal trend (Fig. 2a), while DIP concentrations increased significantly (Fig. 2b). DIN:DIP also showed no significant temporal trend, though DIN:DIP ratios from 2015 to 2019 were among the lowest of the study period, with a mean DIN:DIP of 3.3 (Fig. 2c). Low DIN:DIP values (from 1.2 to 3.6) also occurred in the late 1980s. Durbin-Watson autocorrelation

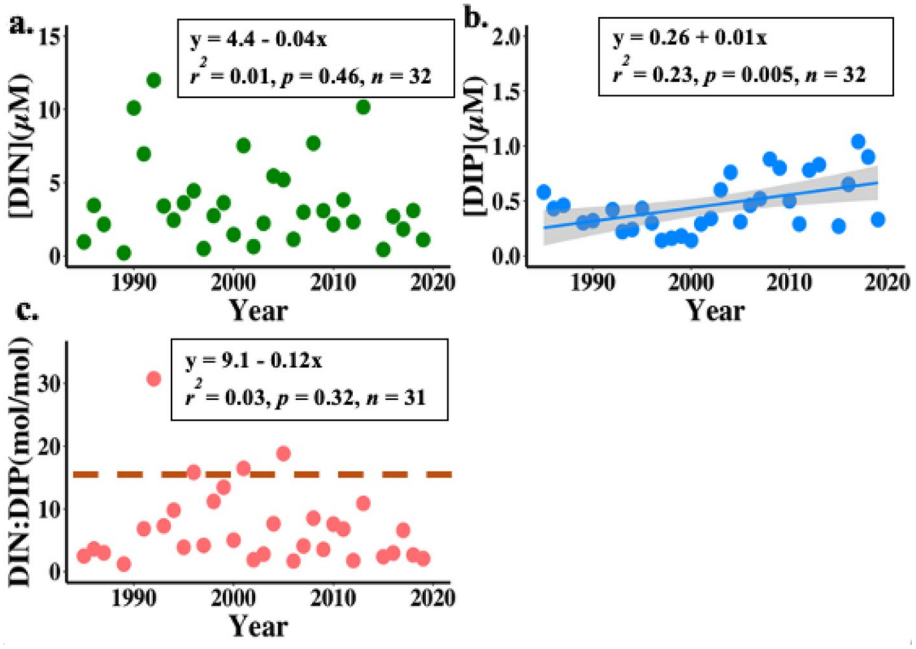

Figure 2. Annual mean NGoM nutrient concentrations 1985 – 2019; (a) DIN (green), (b) DIP (blue), and (c) DIN:DIP (molar ratio, pink). The DIP linear regression was significant and is shown with shaded gray 95% confidence interval. The Redfield ratio of DIN:DIP = 16 is highlighted by a dashed orange line in (c).

tests of annual mean nutrient concentrations over time showed no autocorrelation for annual DIN means over time, and minimal autocorrelation for annual DIP means over time (Table S4). Thus, Cochrane-Orcutt estimations were run on the annual DIP means to transform the data and remove autocorrelation, then Durbin-Watson autocorrelation tests were run again to confirm there was no longer significant autocorrelation. The transformed DIP data had the same r^2 value, p-value, and slope as the untransformed data, and therefore the untransformed data is shown in Fig. 2 for clarity. In addition, the transformation removed heteroscedasticity in the DIP means over time, which was confirmed with the Breusch-Pagan test. Bayesian changepoint analyses of DIN and DIP over time showed that there were no years when there was a significant changepoint in the time series; though there was a decrease in the changepoint time statistic for DIN at 2013 and an increase in the changepoint time statistic for DIP at 1999, the error bars for each were large and included much of the time series (Fig. S5). There were also no significant temporal DIN or DIN:DIP trends in the regional subsets; however, hypoxic and shelf DIP concentrations significantly increased over time (Fig. S6; Table S3).

Annual mean MAR nutrient loading into the NGoM

Similar to NGoM nutrient trends from 1985 to 2019, TDN and DIN loading from the MAR into the NGoM did not change significantly, while DON loading significantly decreased (Fig. 3a, Table S2). Over the same time period, TDP, DIP, and DOP loading from the MAR into the NGoM all increased significantly (Fig. 3b, Table S2). As annual mean MAR discharge did not change significantly over the study time period (Fig. S4b), it is not surprising that MAR DIN concentrations did not show any temporal trend from 1985 to 2019, although MAR DIP concentrations increased significantly (Fig. S4a). Annual mean suspended sediment concentrations, however, declined significantly during the period (Fig. S4c).

Comparing annual mean NGoM DIN and DIP concentrations to MAR discharge, MAR DIN and DIP concentrations, and MAR DIN and DIP loads produced similar patterns of significant relationships for the entire NGoM, the hypoxic region, and the shelf region (Table S4). All were significantly correlated except DIN:DIP, which did not significantly correlate to MAR discharge in the entire NGoM, hypoxic, or shelf regions.

In contrast to results for the hypoxic and shelf regions, correlation analyses for the offshore region found no significant correlations between offshore DIN and MAR discharge, MAR DIN or DIP concentrations or loading (Table S4). On the other hand, offshore DIP concentrations did significantly correlate with MAR discharge, MAR DIP concentrations, and MAR DIN:DIP. Offshore DIN:DIP was significantly correlated to MAR discharge, MAR DIN and DIP concentrations and loading, however, not to MAR DIN:DIP (Table S4). In general, shelf and offshore nutrient concentrations were not significantly correlated with each other over time, with exceptions of the significantly positively correlated offshore DIN:DIP to shelf DIN and DIP concentrations (Table S5).

The areal extent of the hypoxic bottom water in the NGoM fluctuates interannually[35], and correlation analyses were used to determine if this hypoxic area related to nutrient observations. The annual area of hypoxic bottom water was significantly correlated with all forms of N and P loading from the MAR into the NGoM (Table S6). The annual area of hypoxic bottom water was also significantly correlated with annual mean NGoM DIN and DIP concentrations and DIN:DIP in the entire NGoM dataset, the hypoxic region, and the shelf region (Table S6).

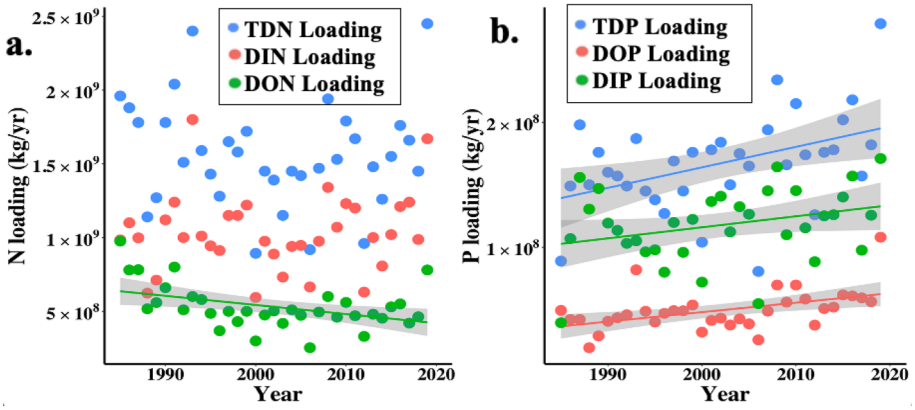

Figure 3. Annual mean (**a**) N loading and (**b**) P loading from the MAR into the NGoM 1985–2019. Non-significant regressions are not shown. Gray shading represents the 95% confidence interval for the statistically significant regression lines. See supplemental Table S1 for corresponding linear regression equations, r^2, *p*-values, and *n*. Based on USGS data (Lee, 2022).

However, the area of hypoxic bottom water was not significantly correlated with offshore nutrient concentrations (Table S6).

Nutrient versus salinity relationships in the NGoM

All NGoM DIN and DIP data (1985–2019) were plotted against corresponding sample salinity in Fig. 4 with each black circle representing a single sample. The conservative mixing function and linear best fits (to ln-transformed values) were also shown. Both DIN and DIP generally declined with increasing salinity, and the slope of the decline was steeper for DIN compared to DIP. Relative to the respective conservative mixing function (shown in purple), only 2% of the DIN values across the salinity range were above the DIN function, while about half (51.8%) of the DIP observations exceeded the DIP mixing function. DIN:DIP in the NGoM generally decreased

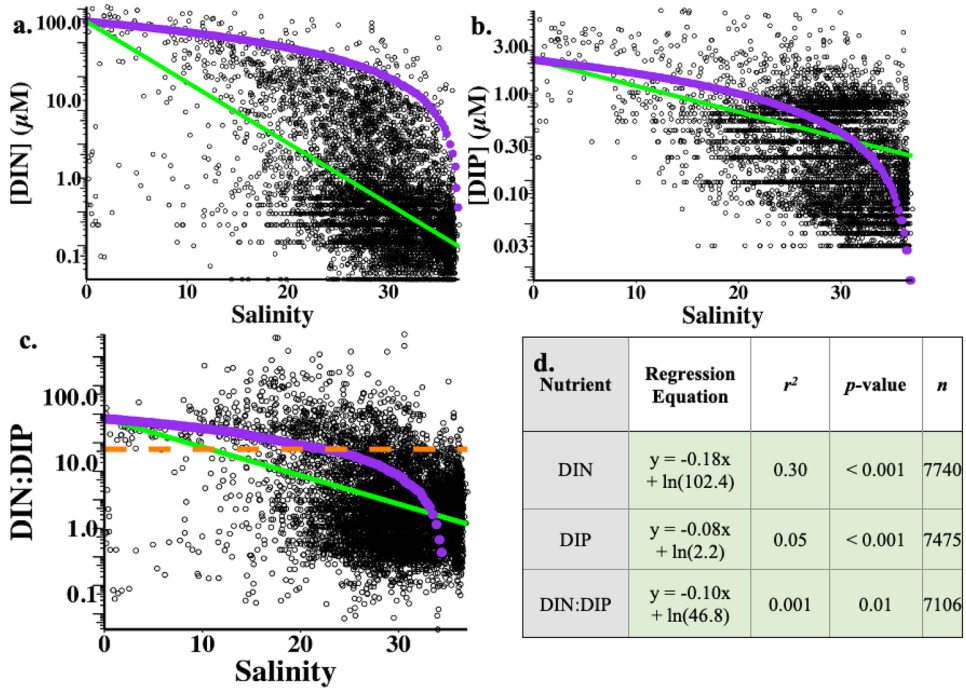

d.

Nutrient	Regression Equation	r^2	*p*-value	*n*
DIN	y = -0.18x + ln(102.4)	0.30	< 0.001	7740
DIP	y = -0.08x + ln(2.2)	0.05	< 0.001	7475
DIN:DIP	y = -0.10x + ln(46.8)	0.001	0.01	7106

Figure 4. NGoM surface nutrient concentration vs. salinity 1985–2019: (a) [DIN]; (b) [DIP]; (c) DIN:DIP. Black circles (excluding 1988 and 2014) represent surface nutrient data in μM for (a) and (b), and are the molar ratio in (c). Untransformed data are shown to facilitate reading values directly from the plots, note the log scale of y-axes. The green lines represent linear regressions to ln-transformed data, with the corresponding equations, r^2, *p*, and *n* values listed in (d). The conservative mixing functions are shown in purple. The dashed orange line in (c) indicates the Redfield ratio of 16 DIN:DIP. Light green shading in (d) highlights significant *p* values.

from above to below the Redfield ratio with increasing salinity, driven by the greater decline in DIN relative to DIP concentrations (Fig. 4c). At 0 salinity in the MAR, DIN:DIP averaged 46.8, and typically declined to less than 16 within the NGoM where salinity was greater than 20.

Nutrient vs. salinity relationships were also plotted separately for the hypoxic, shelf, and offshore subsets of the data (Fig. S7; Table S6). While there were differences in the best-fit slopes for each of the three data subsets, the general patterns were similar to the overall data set. Changing the freshwater endmember across the range of DIN and DIP values from 1985 to 2019 did not affect nutrient vs. salinity relationships. For all regions, DIN declined more for a given change in salinity than DIP, and a much larger fraction of the DIP observations (relative to the DIN observations) exceeded the mixing function. Subsequent analyses subset the data shown in Fig. 4 to examine the residuals of each nutrient from the mixing functions.

Nutrient residuals relative to the conservative mixing function were calculated for each data point as the difference between actual and predicted value, with positive residuals meaning an excess or production of the nutrient while the negative residuals indicate the loss or consumption of the nutrient in addition to dilution by low-nutrient ocean water (depending on the sample salinity; Fig. 5, Figs. S8, S9). Here, we emphasize the presentation of data on the DIP residuals because over half exceeded the mixing function, in contrast to only 2% of DIN residuals. Residuals were shown relative to the DIP mixing function ($y = -0.06x + 2.2$) which is zero on the y-axis. Additionally, the symbol colors reflect residual values relative to both DIP and TDP ($y = -0.09x + 3.3$) mixing functions, under the assumption that all TDP from the MAR could be converted to DIP in the NGoM.

Discussion

Over time, DIP concentrations significantly increased in the NGoM, but with greater interannual variability over time. This rise in DIP was notable not only because of its increase over time, but also because DIP concentrations were frequently in excess of the MAR DIP mixing function across the salinity gradient. Even when we used annual values of MAR DIP concentrations, about half of the NGoM DIP concentrations still exceeded the mixing line. Thus, although MAR DIP loading rose over time, it was insufficient to explain the distribution of DIP concentrations in the NGoM. This contrasts to MAR DIN values, which could account for NGoM DIN concentrations along the salinity gradient because DIN concentrations were predominantly (98%) below the MAR DIN mixing function. Other studies have similarly proposed that there are excess sources of DIP (or selective removal of DIN) in the NGoM shelf region beyond the average MAR outflow area[60,68].

A two-endmember mixing model for NGoM nutrient distributions is highly simplified and inputs from freshwater endmembers other than the MAR certainly contribute to NGoM nutrient concentrations[69]. Nevertheless, the high relative contribution of the MAR to NGoM nutrient loading[32] and the temporal correlations between MAR nutrient loads and NGoM concentrations shown in this study support our focus on the MAR as the dominant freshwater endmember. Moreover, this two-endmember approximation does effectively highlight fundamental differences in the spatial and temporal patterns of DIN and DIP in the NGoM that require further exploration. Resolving the NGoM DIP-salinity relationship requires a process that provides DIP to the NGoM in excess of the MAR DIP source along the entire salinity gradient, that also increases through time, at least over the shelf region. In this context it is worth highlighting that the slopes of DIN, DIP, and DIN:DIP vs. salinity are nearly identical across the hypoxic, shelf, and offshore regions, suggesting that the same processes control nutrient patterns regardless of distance from shore, or bottom depth. Within the MAR DIP plume itself, relevant processes to consider include DIP regeneration and recycling, precipitation and aerosols, adsorption/desorption of P from suspended particles and benthic sediment, vertical mixing, and DOP mineralization.

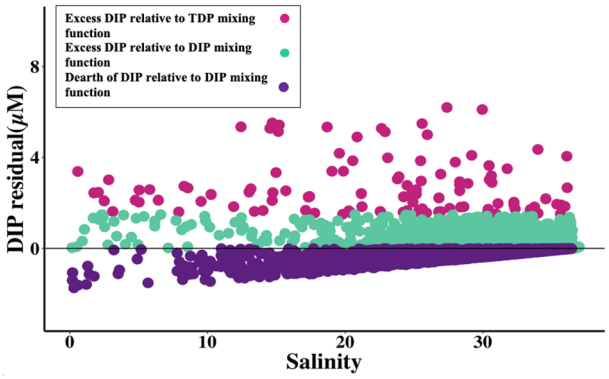

Figure 5. Residuals of NGoM DIP concentrations (1985–2019) relative to the conservative mixing functions connecting MAR DIP and TDP to the offshore endmember. Each point equates to an individual sample and shows the DIP residual relative to the MAR DIP mixing function ($y = -0.059x + 2.2$). Positive residuals (teal and pink) indicate that the actual values were higher than predicted, and negative residuals (purple) signify that the actual values were lower than predicted by the MAR DIP mixing function. Pink values are positive relative to both the MAR DIP mixing function and would also be positive relative to the MAR TDP mixing function ($y = -0.089x + 3.3$). Teal values are positive relative to the MAR DIP mixing function, but would be negative relative to the MAR TDP mixing function. Purple values are negative relative to both mixing functions.

DIP regeneration/recycling, the conversion of autochthonous organic P to DIP[6], is an important source of P to NGoM phytoplankton, and P turnover times within the upper water column are rapid[70]. However, such cycling cannot by itself explain NGoM DIP concentrations that surpass the MAR DIP mixing function since regeneration of DIP from the MAR would need additional DIP sources to exceed mixing. Throughout the MAR watershed and NGoM, P is deposited from rainfall, dust, and anthropogenic emissions[71,72]. While atmospheric P deposition has increased over time in other locations[73], the atmospheric DIP and TP contribution to the NGoM is still very small (2–10 ng m^{-3})[74].

DIP adsorbs to particles in freshwater, and is released with increasing salinity and discharge[69,75]. However, suspended-sediment-derived P is unlikely to explain the upward trend in NGoM DIP, because the percentage of P in MAR suspended sediment stayed relatively stable over time (Fig. S4d), while MAR suspended sediment concentrations have significantly declined since 1985. P can also be remobilized into bottom waters from benthic iron or sulfate reduction, mediated by oxygen levels[76,77]. For example, during NGoM hypoxic events, TDP is released into the water column from bottom sediments[7]. Though benthic DIP sources are likely important within the MAR watershed and in shallow, nearshore areas of the NGoM[69], our results show a pattern of excess DIP at high salinities, that are typically found over deep water columns, further offshore.

Although stratification in the NGoM can be strong[78], the two-endmember model applied to the nutrient distributions implies continuous vertical or horizontal mixing between the endmembers. While vertical mixing transports DIP to the surface from deeper depths, it also transports DIN. To provide excess DIP to the NGoM system, the deeper waters being mixed upwards would need to have lower DIN:DIP than the offshore endmember. In addition, to align with the temporal trend in DIP, there would need to be an increase in either the mixing intensity over time, or a decrease in DIN:DIP in those deeper waters. Further research will be needed to assess these possibilities.

Biological mineralization of organic P compounds through enzymatic reactions[12,79] or photolysis[80] could break down organic P-containing compounds originally delivered from the MAR, adding DIP to the NGoM water column in excess of the MAR DIP mixing function. Figure 5 demonstrates that including MAR TDP inputs would be sufficient to explain most NGoM DIP concentrations if all MAR-derived DOP was converted into DIP along the salinity gradient in the NGoM. Thus, the combination of DOP and DIP loading from the MAR could account for increasing DIP concentrations in the NGoM, though other processes are not excluded. While it seems unlikely that all MAR-derived DOP would be converted to DIP, the match with the DIP data suggests that DOP mineralization is an important source of DIP along the salinity gradient. Further research quantifying the fraction and processes of MAR DOP mineralization along the salinity gradient would help constrain the degree to which MAR DOP inputs can explain NGoM DIP trends.

This study expands upon previous nutrient research in the MAR and NGoM. From 1985 to 2019, N and P loading in the MAR increased greatly relative to the 1950s[33,36]. During the period of this study, DIN loading fluctuated around a value of approximately 1×10^9 kg yr^{-1}, while DON loading decreased significantly by approximately 20% from 1985 to 2019. Stabilization of DIN loads[60] and decreasing DON loads could reflect upstream N management (e.g., changing N fertilizer application timing)[55]. Conversely, MAR DIP and DOP loading significantly increased from 1985 to 2019, contrasting with conclusions from studies based on earlier data[40]. Similar to many other NGoM nutrient studies, the NGoM surface nutrient data set is dominated by samples collected in the summer months (Fig. S2).

Increases in P in the MAR watershed could come from myriad sources over time, since the watershed covers almost half the contiguous US states. Though P additions have been somewhat curtailed from wastewater treatment and industry, agriculture (i.e., pesticides, herbicides, and fertilizers) is still a sizeable source of extremely high P inputs to the MAR[81,82]. Long-lived organic P species that are used in many pesticides, herbicides, and fertilizers have the potential to persist in water and soil and act as a source of P that accumulates and is remobilized and recycled over long timescales[83]. In addition, legacy nutrients stored in soils and reservoirs continually leach into the MAR watershed, and though legacy nutrient sources have been well studied for N[13], the magnitude and residence times for legacy P pools are harder to model and measure[14,83].

In the MAR, although there were clear temporal trends in DON loading and all forms of P loading, there was also considerable interannual variability. While MAR DIN and DIP concentrations varied by approximately a factor of 2 interannually, MAR discharge ranged across nearly an order of magnitude over the same time period. MAR mean discharge in 2019 was by far the highest of our study period, and also contributed the highest mean annual TDN and TDP loading since 1985. Prior studies have highlighted that much of the interannual variability in MAR nutrient fluxes can be attributed to interannual variability in precipitation across the MAR watershed[55,64,75]. For example, 50 to 67% of the interannual variation in MAR N fluxes is accounted for by river discharge alone[60,84]. In turn, MAR watershed precipitation and discharge has been shown to correlate with the El Niño Southern Oscillation and the Atlantic Multidecadal Oscillation (AMO)[34,56,60].

In addition, during high flow years in which MAR spillways (e.g., Morganza, Bonnet Carré) were opened, nutrient dynamics and location of freshwater delivery to the NGoM fundamentally change. The Bonnet Carré spillway diverts water from the Mississippi River into Lake Ponchartrain, which then connects to the NGoM, resulting in lower concentrations of suspended sediment, TDN, TDP, DIN, and DIN:DIP, and higher DON content[85]. Openings of the Bonnet Carré spillway in 1997, 2008, 2011, 2016, 2018, and 2019[86,87], coincided with low NGoM DIN:DIP in our study. However, it is difficult to assess the relative importance of spillway openings, versus general increased flow, on nutrient trends.

Significant positive temporal correlations between MAR nutrients, MAR loading, and MAR discharge, and NGoM nutrient concentrations and ratios indicated that processes within the MAR watershed, especially influences on discharge, contributed significantly to interannual variability in NGoM surface nutrients, though with decreasing influence toward the offshore region. Similarly, Lehrter et al. (2009) found that the influence of MAR discharge on chlorophyll concentration and primary productivity diminishes across the broader shelf. In the

offshore region, interannual variability in DIP concentrations remained significantly correlated to MAR discharge, MAR DIP concentrations, and MAR DIN:DIP, while interannual variability of offshore DIN concentrations was not significantly correlated to the MAR observations. Thus, links between riverine inputs and offshore DIP concentrations were stronger than for offshore DIN, consistent with greater nearshore N retention[60,88].

As mentioned above, the rise in MAR DIN loading and consequent nearshore hypoxia in the NGoM observed from the 1950s to the 1980s[35,36,89] seems to have stabilized during the period of this study. More recently, Karnauskas et al. (2015) suggested that an ecosystem-wide reorganization of the NGoM occurred in the mid-1990s as a result of physical ecosystem changes driven by the AMO; which was in a cool phase from the 1970s to the 1990s, and in a warm phase from the mid-1990s to at least the mid-2000s. The AMO warm phase decreased rainfall, MAR discharge, and mixed layer depth[56]. Some observations in this study may relate to the AMO because in the mid-1990s, annual mean NGoM DIN and DIP concentrations decreased from earlier values, resulting in DIN:DIP close to and below 16; especially in the offshore region, where DIN and DIP concentrations were extremely low. In the early 2000s, DIN and DIP concentrations began to rebound. If the AMO sets the stage for the processes that control nutrient distributions in the NGoM, as the AMO returns to a cool phase[90] then we would expect DIP to again fall.

An extensive analysis of NGoM surface nutrient data from 1985 to 2012 by Cardona et al. (2016) suggested that there was an increase in surface DIN and DIP utilization from 2010 to 2011, possibly connected to the Deepwater Horizon oil spill, or to an exceptional deep winter mixed layer[31]. With the advantage of additional years of observations, the NGoM nutrient conditions from 2010 to 2012 appear to have only been a temporary shift, as the prior conditions recurred post-2013. It remains to be seen whether the long-term increase in DIP concentrations throughout the NGoM described in this study will lead to a longer-term shift in nutrients.

Nutrient concentrations influence and correlate with phytoplankton biomass, community composition, and spatial variance in chlorophyll-*a* concentrations throughout the NGoM[91,92]. In this study, we showed that surface DIP concentrations in the NGoM increased over time, while DIN did not. This increase in DIP relative to DIN has implications for nutrient limitation of phytoplankton growth and production, especially since the system has been classified as both P and N limited through time[11]. While phytoplankton in the NGoM have been described as predominantly N limited[11,31,52], transient P limitation (and higher DIN:DIP) has been observed in spring and summer months in the MAR plume and nearshore region of the NGoM[42,70,92]. In general, N limitation typically occurs with N concentrations lower than 1 μM and N:P less than 10, while P limitation commonly is associated with N:P greater than 30[47,93,94], though empirical results sometimes deviate from the predictions of these criteria[95]. Nevertheless, applying these nutrient ratio criteria, data in this study suggest P limitation is plausible throughout the salinity gradient in the NGoM, though the conditions for N limitation are more likely at high salinities and in the offshore region[45]. Meanwhile, the temporal increase in NGoM DIP concentrations suggests more frequent and pervasive N limitation of phytoplankton over time. P limitation at low salinities has the potential to lessen the effect of eutrophication on bottom water oxygen concentrations and reduce the incidence and strength of NGoM hypoxia[54]. Increasing excess P may therefore increase the occurrence and severity of NGoM hypoxia.

N fixation should be favored in N-limited surface waters with ample light and high DIP concentrations[96]. Given increasing likelihood of N limitation and P availability, the suitability of the NGoM for N fixation may have increased during the 1985 to 2019 time period[97]. If this trend continues, increased N fixation in the NGoM should also enhance C sequestration within the NGoM, as has been proposed for other areas affected by river plumes[98].

Nutrients in both the MAR and the NGoM have changed over the last 35 years. In the MAR, N loading stabilized and P loading significantly increased since 1985. In the NGoM, DIP concentrations increased over time, while DIN concentrations did not. These changes were primarily driven by trends in the shelf region, as opposed to further offshore. Increases in MAR DIP loading by itself could not explain the distribution of NGoM DIP with salinity. MAR TDP loading would be sufficient to account for spatial and temporal DIP patterns in the NGoM, but only if all MAR DOP was converted to DIP by enzymatic reactions and/or photolysis. Anomalous nutrient conditions from 2010 to 2012 did not persist. Nevertheless, the increasing likelihood of N limitation and excess P availability in the NGoM has implications for phytoplankton communities, diazotrophy, and the prevalence and extent of nearshore hypoxia.

Data availability

The datasets generated during and analyzed during the current study are available from the corresponding author on reasonable request. All compiled data sources are included in the Supplementary Table S1. MAR nutrient concentration data were compiled from USGS, and nutrient loads were sourced from USGS Load Estimation (LOADEST) and Weighted Regressions on Time, Discharge, and Season method (WRTDS) USGS data (Lee, 2022) from St. Francisville, LA, USA (USGS 07373420 Hydrologic Unit 08070100).

Received: 20 October 2023; Accepted: 25 March 2024
Published online: 27 March 2024

References

1. Redfield, A. C. The biological control of chemical factors in the environment. *Am. Sci.* **46**, 205–221 (1958).
2. Howarth, R. Nutrient limitation of net primary production in marine ecosystems. *Annu. Rev. Ecol. Syst.* **19**, 89–100 (1988).
3. Moore, C. M. *et al.* Processes and patterns of oceanic nutrient limitation. *Nat. Geosci.* **6**, 701–710 (2013).
4. Vitousek, P. M. & Howarth, R. W. Nitrogen limitation on land and in the sea: How can it occur?. *Biogeochemistry* **13**, 87–115 (1991).
5. Tyrrell, T. The relative influences of nitrogen and phosphorus on oceanic primary production. *Nature* **400**, 525–531 (1999).
6. Benitez-Nelson, C. R. The biogeochemical cycling of phosphorus in marine systems. *Earth Sci. Rev.* **51**, 109–135 (2000).
7. Adhikari, P. L., White, J. R., Maiti, K. & Nguyen, N. Phosphorus speciation and sedimentary phosphorus release from the Gulf of Mexico sediments: Implication for hypoxia. *Estuar. Coast. Shelf Sci.* **164**, 77–85 (2015).

8. Geider, R. J. & La Roche, J. Redfield revisited: variability of C:N: P in marine microalgae and its biochemical basis. *Eur. J. Phycol.* **37**, 1–17 (2002).
9. Zehr, J. P. & Capone, D. G. Changing perspectives in marine nitrogen fixation. *Science* https://doi.org/10.1126/science.aay9514 (2020).
10. Carstensen, J. *et al.* Hypoxia in the Baltic Sea: Biogeochemical cycles, benthic fauna, and management. *Ambio* **43**, 26–36 (2014).
11. Turner, R. E. & Rabalais, N. N. Nitrogen and phosphorus phytoplankton growth limitation in the Northern Gulf of Mexico. *Aquat. Microb. Ecol.* **68**, 159–169 (2013).
12. Duhamel, S. *et al.* Phosphorus as an integral component of global marine biogeochemistry. *Nat. Geosci.* **14**, 359–368 (2021).
13. Van Meter, K. J., Basu, N. B. & Van Capellen, P. Two centuries of nitrogen dynamics: Legacy sources and sinks in the Mississippi and Susquehanna River Basins. *Glob. Biogeochem. Cycles* **31**, 2–23 (2017).
14. McCrackin, M. L. *et al.* A century of legacy phosphorus dynamics in a large Drainage Basin. *Glob. Biogeochem. Cycles* **32**, 1107–1122 (2018).
15. Rabalais, N. N. *et al.* Nutrient-enhanced productivity in the Northern Gulf of Mexico: Past, present and future. In *Geological Society Special Publication* 39–63 (2002). https://doi.org/10.1007/978-94-017-2464-7_4.
16. Fennel, K. & Laurent, A. N and P as ultimate and proximate limiting nutrients in the Northern Gulf of Mexico: Implications for hypoxia reduction strategies. *Biogeosciences* **15**, 3121–3131 (2018).
17. Redfield, A.C. On the proportions of organic derivatives in sea water and their relation to the composition of plankton. James Johnstone Memorial Volume. *Univ. Press Liverp.* 176–192 (1934).
18. Downing, J. A. Marine nitrogen: Phosphorus stoichiometry and the global N: P cycle. *Biogeochemistry* **37**, 237–252 (1997).
19. Turner, R. E., Rabalais, N. N., Justic, D. & Dortch, Q. Global patterns of dissolved N, P and Si in large rivers. *Biogeochemistry* **64**, 297–317 (2003).
20. Wang, W. L., Moore, J. K., Martiny, A. C. & Primeau, F. W. Convergent estimates of marine nitrogen fixation. *Nature* **566**, 205–2011 (2019).
21. Nausch, M. & Nausch, G. Phosphorus speciation and transformation along transects in the Benguela upwelling region. *J. Mar. Syst.* **140**, 111–112 (2014).
22. Martiny, A. C. *et al.* Biogeochemical controls of surface ocean phosphate. *Sci. Adv.* **5**, 341–369 (2019).
23. Cochrane, J. D. & Kelly, F. Low-frequency circulation on the Texas-Louisiana continental shelf. *J. Geophys. Res.* **91**, 10645–10655 (1986).
24. Wiseman, W. J. & Garvine, R. W. Plumes and coastal currents near large river mouths. *Estuaries* **18**, 509–517 (1995).
25. Dagg, M., Benner, R., Lohrenz, S. & Lawrence, D. Transformation of dissolved and particulate materials on continental shelves influenced by large rivers: Plume processes. *Cont. Shelf Res.* **24**, 833–858 (2004).
26. Walker, N. D., Wiseman, W. J., Rouse, L. J. & Babin, A. Effects of River discharge, wind stress, and slope eddies on circulation and the satellite-observed structure of the Mississippi River Plume. *J. Coast. Res.* **21**, 1228–1244 (2005).
27. Schiller, R. V., Kourafalou, V. H., Hogan, P. & Walker, N. D. The dynamics of the Mississippi River plume: Impact of topography, wind and offshore forcing on the fate of plume waters. *J. Geophys. Res. Oceans* **116**, 6029 (2011).
28. Hitchcock, G. L. *et al.* Property fields in an effluent plume of the Mississippi river. *J. Mar. Syst.* **12**, 109–126 (1997).
29. Morey, S. L. *et al.* Export pathways for river discharged fresh water in the Northern Gulf of Mexico. *J. Geophys. Res. Oceans* **108**, 3303 (2003).
30. Rabalais, N. N., Turner, R. E., Wiseman, W. J. & Boesch, D. F. A brief summary of hypoxia on the Northern Gulf of Mexico continental shelf: 1985–1988. *Geol. Soc. Spec. Publ.* **58**, 35–47 (1991).
31. Cardona, Y. *et al.* Highly variable nutrient concentrations in the Northern Gulf of Mexico. *Deep-Sea Res. Part II Top. Stud. Oceanogr.* **129**, 20–30 (2016).
32. Fry, B. *et al.* Carbon Dynamics on the louisiana continental shelf and cross-shelf feeding of Hypoxia. *Estuaries Coasts* **38**, 703–721 (2015).
33. Rabalais, N. N. & Turner, R. E. Oxygen depletion in the gulf of Mexico adjacent to the Mississippi river. *Past Present Water Column Anoxia* **70**, 73–78 (2006).
34. Gomez, F. A. *et al.* ENSO-induced co-variability of Salinity, Plankton biomass and coastal currents in the Northern Gulf of Mexico. *Sci. Rep.* **9**, 1–10 (2019).
35. Rabalais, N. N. & Turner, R. E. Gulf of Mexico Hypoxia: Past, present, and future. *Limnol. Oceanogr. Bull.* **28**, 117–124 (2019).
36. Turner, R. E. & Rabalais, N. N. Changes in Mississippi River water quality this century. *BioScience* **41**, 140–147 (1991).
37. David, M. B., Drinkwater, L. E. & McIsaac, G. F. Sources of nitrate yields in the Mississippi River Basin: Sources of nitrate yields in the Mississippi River Basin. *J. Environ. Qual.* **39**, 1657–1667 (2010).
38. Rabalais, N. N. *et al.* Nutrient changes in the Mississippi River and system responses on the adjacent continental shelf. *Estuaries* **19**, 386–407 (1996).
39. Stets, E. G., Kelly, V. J. & Crawford, C. G. Regional and temporal differences in nitrate trends discerned from long-term water quality monitoring data. *J. Am. Water Resour. Assoc.* **51**, 1394–1407 (2015).
40. Goolsby, D. A., *et al.* Flux and sources of nutrients in the Mississippi-Atchafalaya River Basin: Topic 3 Report for the Integrated Assessment on Hypoxia in the Gulf of Mexico. Item Type monograph. In *Rep. Integr. Assess. Hypoxia Gulf Mex. NOAA Coast. Ocean Program Decis. Anal. Ser.* **17**, (1999).
41. Seitzinger, S. P. *et al.* Global river nutrient export: A scenario analysis of past and future trends. *Glob. Biogeochem. Cycles* https://doi.org/10.1029/2009GB003587 (2010).
42. Sylvan, J. B. *et al.* Phosphorus limits phytoplankton growth on the Louisiana shelf during the period of hypoxia formation. *Environ. Sci. Technol.* **40**, 7548–7553 (2006).
43. Sylvan, J. B., Quigg, A., Tozzi, S. & Ammerman, J. W. Eutrophication-induced phosphorus limitation in the Mississippi River plume: Evidence from fast repetition rate fluorometry. *Limnol. Oceanogr.* **52**, 2679–2685 (2007).
44. Quigg, A. *et al.* Going west: Nutrient limitation of primary production in the Northern Gulf of Mexico and the importance of the Atchafalaya River. *Aquat. Geochem.* **17**, 519–544 (2011).
45. Lohrenz, S. E., Dagg, M. J. & Whitledge, T. E. Enhanced primary production at the plume/oceanic interface of the Mississippi River. *Cont. Shelf Res.* **10**, 639–664 (1990).
46. Lohrenz, S. E., Fahnenstiel, G. L. & Redalje, D. G. Nutrients, irradiance, and mixing as factors regulating primary production in coastal waters impacted by the Mississippi River plume. *Cont. Shelf Res.* **19**(9), 1113–1141 (1999).
47. Wysocki, L. A., Bianchi, T. S., Powell, R. T. & Reuss, N. Spatial variability in the coupling of organic carbon, nutrients, and phytoplankton pigments in surface waters and sediments of the Mississippi River plume. *Estuar. Coast. Shelf Sci.* **69**, 47–63 (2006).
48. Rabalais, N. N. *et al.* Hypoxia in the Gulf of Mexico. *J. Environ. Qual.* **30**, 320–329 (2001).
49. Eadie, B. J. *et al.* Records of nutrient-enhanced coastal ocean productivity in sediments from the Louisiana continental shelf. *Estuaries* **17**, 754–765 (1994).
50. Parsons, M. L. & Dortch, Q. Sedimentological evidence of an increase in Pseudo-nitzschia (Bacillariophyceae)abundance in response to coastal eutrophication. *Limnol. Oceanogr.* **47**, 551–558 (2002).
51. Lehrter, J. C., Murrell, M. C. & Kurtz, J. C. Interactions between freshwater input, light, and phytoplankton dynamics on the Louisiana continental shelf. *Cont. Shelf Res.* **29**, 1861–1872 (2009).

52. Turner, R. E., Rabalais, N. N., Alexander, R. B., Mcisaac, G. & Howarth, R. W. Characterization of nutrient, organic carbon, and sediment loads and concentrations from the Mississippi River into the Northern Gulf of Mexico. *Estuaries Coasts* **30**, 773–790 (2007).
53. Greene, R. M., Lehrter, J. C. & Hagy, J. D. Multiple regression models for hindcasting and forecasting midsummer hypoxia in the Gulf of Mexico. *Ecol. Appl.* **19**, 1161–1175 (2009).
54. Laurent, A. & Fennel, K. Simulated reduction of hypoxia in the Northern Gulf of Mexico due to phosphorus limitation. *Elem. Sci. Anthr.* https://doi.org/10.12952/journal.elementa.000022 (2014).
55. Lu, C. *et al.* Increased extreme precipitation challenges nitrogen load management to the Gulf of Mexico. *Nat. Commun. Earth Environ.* https://doi.org/10.1038/s43247-020-00020-7 (2020).
56. Karnauskas, M. *et al.* Evidence of climate-driven ecosystem reorganization in the Gulf of Mexico. *Glob. Change Biol.* **21**, 2554–2568 (2015).
57. Pante, E. & Simon-Bouhet, B. marmap: A package for importing, plotting and analyzing bathymetric and topographic data in R. *PLoS ONE* **8**, e73051 (2013).
58. Goolsby, D. A., Battaglin, W. A., Aulenbach, B. T. & Hooper, R. P. Nitrogen input to the Gulf of Mexico. *J. Environ. Qual.* **30**, 329–336 (2001).
59. Wawrik, B., Paul, J. H., Bronk, D. A., John, D. & Gray, M. High rates of ammonium recycling drive phytoplankton productivity in the offshore Mississippi River plume. *Aquat. Microb. Ecol.* **35**, 175 (2004).
60. Lohrenz, S. E., Redalje, D. G., Cai, W. J., Acker, J. & Dagg, M. A retrospective analysis of nutrients and phytoplankton productivity in the Mississippi River plume. *Cont. Shelf Res.* **28**, 1466–1475 (2008).
61. Lee, C. J. Nutrient loads to the Gulf of Mexico produced by the USGS national water quality network, 1968–2021. (2022).
62. U.S. Geological Survey. National Water Information System data (USGS Water Data for the Nation). (2022).
63. Goolsby, D. A., Battaglin, W. A., Aulenbach, B. T. & Hooper, R. P. Nitrogen flux and sources in the Mississippi River Basin. *Sci. Total Environ.* **248**, 75–86 (2000).
64. Donner, S. D. & Scavia, D. How climate controls the flux of nitrogen by the Mississippi River and the development of hypoxia in the Gulf of Mexico. *Limnol. Oceanogr.* **52**, 856–861 (2007).
65. Lee, C. J., Murphy, J. C., Crawford, C. G. & Deacon, J. R. Methods for computing water-quality loads at sites in the U.S. Geological Survey National Water Quality Network. (2017).
66. Cael, B. B., Bisson, K., Boss, E., Dutkiewicz, S. & Henson, S. Global climate-change trends detected in indicators of ocean ecology. *Nature* **619**, 551–554 (2023).
67. Walker, N. D. Satellite assessment of Mississippi River plume variability: causes and predictability. *Remote Sens. Environ.* **58**, 21–35 (1996).
68. Bargu, S. *et al.* Mississippi River diversions and phytoplankton dynamics in deltaic Gulf of Mexico estuaries: A review. *Estuar. Coast. Shelf Sci.* **221**, 39–52 (2019).
69. He, S. & Xu, Y. J. Phosphorus fluxes from three coastalwatersheds under varied agriculture intensities to the Northern Gulf of Mexico. *Water Switz.* **10**, 816 (2018).
70. Popendorf, K. & Duhamel, S. Variable phosphorus uptake rates and allocation across microbial groups in the oligotrophic Gulf of Mexico. *Environ. Microbiol.* **17**, 3992–4006 (2015).
71. Walsh, J. J. *et al.* Red tides in the Gulf of Mexico: Where, when, and why?. *J. Geophys. Res.* https://doi.org/10.1029/2004JC002813 (2006).
72. Migon, C. & Sandroni, V. Phosphorus in rainwater: Partitioning inputs and impact on the surface coastal ocean. *Limnol. Oceanogr.* **44**, 1160–1165 (1999).
73. Pan, Y. *et al.* Enhanced atmospheric phosphorus deposition in Asia and Europe in the past two decades. *Atmos. Ocean. Sci. Lett.* **14**, 100051 (2021).
74. Mahowald, N. *et al.* Global distribution of atmospheric phosphorus sources, concentrations and deposition rates, and anthropogenic impacts. *Glob. Biogeochem. Cycles* https://doi.org/10.1029/2008GB003240 (2008).
75. Tan, Z. *et al.* Increased extreme rains intensify erosional nitrogen and phosphorus fluxes to the Northern Gulf of Mexico in recent decades. *Environ. Res. Lett.* **16**, 054080 (2021).
76. Sutula, M., Bianchi, T. S. & Mckee, B. A. Effect of seasonal sediment storage in the lower Mississippi River on the flux of reactive particulate phosphorus to the Gulf of Mexico. *Limnol. Oceanogr.* **49**, 2223–2235 (2004).
77. Ding, S. *et al.* In situ, high-resolution evidence for iron-coupled mobilization of phosphorus in sediments. *Sci. Rep.* **6**, 1–11 (2016).
78. Obenour, D. R., Michalak, A. M., Zhou, Y. & Scavia, D. Quantifying the impacts of stratification and nutrient loading on hypoxia in the Northern Gulf of Mexico. *Environ. Sci. Technol.* **46**, 5489–5496 (2012).
79. Paytan, A. & McLaughlin, K. The oceanic phosphorus cycle. *Chem. Rev.* **107**, 563–576 (2007).
80. Karl, D. M. & Björkman, K. Dynamics of dissolved organic phosphorus. In *Biogeochemistry of Marine Dissolved Organic Matter* 233–334 (Burlington Academic Press, 2015).
81. Hébert, M. P., Fugère, V. & Gonzalez, A. The overlooked impact of rising glyphosate use on phosphorus loading in agricultural watersheds. *Front. Ecol. Environ.* **17**, 48–56 (2019).
82. Turner, R. E., Milan, C. S., Swenson, E. M. & Lee, J. M. Peak chlorophyll a concentrations in the lower Mississippi River from 1997 to 2018. *Limnol. Oceanogr.* **67**, 703–712 (2022).
83. Sharpley, A. *et al.* Phosphorus legacy: Overcoming the effects of past management practices to mitigate future water quality impairment. *J. Environ. Qual.* **42**, 1308–1326 (2013).
84. McIsaac, G. F., David, M. B., Gertner, G. Z. & Goolsby, D. A. Relating net nitrogen input in the Mississippi River Basin to nitrate flux in the lower Mississippi River. *J. Environ. Qual.* **31**, 1610–1622 (2002).
85. Lane, R. R., Day, J. W., Kemp, G. P. & Demcheck, D. K. The 1994 experimental opening of the Bonnet Carre Spillway to divert Mississippi River water into Lake Pontchartrain, Louisiana. *Ecol. Eng.* **17**, 411–422 (2001).
86. Parra, S. M. *et al.* Bonnet Carré Spillway freshwater transport and corresponding biochemical properties in the Mississippi Bight. *Cont. Shelf Res.* **199**, 104114 (2020).
87. U.S. Army Corps of Engineers. Spillway Operation Information (2019).
88. Howe, S., Miranda, C., Hayes, C. T., Letscher, R. T. & Knapp, A. N. The dual isotopic composition of nitrate in the gulf of Mexico and Florida straits. *J. Geophys. Res. Oceans* **125**, e2020JC016047 (2020).
89. Turner, R. E., Rabalais, N. N. & Justic, D. Gulf of Mexico hypoxia: Alternate states and a legacy. *Environ. Sci. Technol.* **42**, 2323–2327 (2008).
90. Frajka-Williams, E., Beaulieu, C. & Duchez, A. Emerging negative Atlantic Multidecadal Oscillation index in spite of warm subtropics. *Sci. Rep.* **7**, 11224 (2017).
91. Chen, X., Lohrenz, S. E. & Wiesenburg, D. A. Distribution and controlling mechanisms of primary production on the Louisiana-Texas continental shelf. *J. Mar. Syst.* **25**, 179–207 (2000).
92. Qian, Y., Jochens, A. E., Kennicutt, M. C. & Biggs, D. C. Spatial and temporal variability of phytoplankton biomass and community structure over the continental margin of the northeast Gulf of Mexico based on pigment analysis. *Cont. Shelf Res.* **23**, 1–17 (2003).
93. Dortch, Q. & Whitledge, T. E. Does nitrogen or silicon limit phytoplankton production in the Mississippi River plume and nearby regions?. *Cont. Shelf Res.* **12**, 1293–1309 (1992).

94. Goldman, J. C., McCarthy, J. J. & Peavey, D. G. Growth rate influence on the chemical composition of phytoplankton in oceanic waters. *Nature* **279**, 210–215 (1979).
95. Juhl, A. & Murrell, M. Nutrient limitation of phytoplankton growth and physiology in a subtropical estuary (Pensacola Bay, Florida). *Bull. Mar. Sci.* **82**(1), 59–82 (2008).
96. Gruber, N. Elusive marine nitrogen fixation. *Proc. Natl. Acad. Sci. U.S.A.* **113**, 4246–4248 (2016).
97. Mulholland, M. R., Berhardt, P. W., Heil, C. A., Bronk, D. A. & O'Neil, J. M. Nitrogen fixation and release of fixed nitrogen by *Trichodesmium* spp. in the Gulf of Mexico. *Limnol. Oceanogr.* **51**, 1762–1776 (2006).
98. Subramaniam, A. *et al.* Amazon River enhances diazotrophy and carbon sequestration in the tropical North Atlantic Ocean. *Proc. Natl. Acad. Sci. U.S.A.* **105**, 10460–10465 (2008).

Acknowledgements

This study was supported by National Science Foundation award 1737240. We thank the captain and crew aboard R/V Endeavor on cruises EN620 and EN642. We thank Benjamin Ramcharitar, Nicholas Bock, Ella Steiger, and John Richardson for their help with collection and analyses, Annalisa Bracco and Yuley Cardona for their gracious sharing of data and guidance. We also thank Chief Scientist Joe Montoya, Anna Martin, and Erica Strope. We sincerely thank and are grateful to all the teams that collected and processed all of the historical samples used in this study.

Author contributions

K.A. contributed to conceptualization, methodology, formal analysis, investigation, data curation, writing original draft, writing, review, and editing, and visualization. A.R.J. contributed to conceptualization, methodology, resources, writing original draft, writing, review, and editing, supervision, project administration, and funding acquisition. A.S. and S.D. contributed to conceptualization, writing, review, and editing, and funding acquisition. All authors approved the submitted version.

Competing interests

The authors declare no competing interests.

Additional information

Supplementary Information The online version contains supplementary material available at https://doi.org/10.1038/s41598-024-58044-4.

Correspondence and requests for materials should be addressed to K.G.A.

Reprints and permissions information is available at www.nature.com/reprints.

Publisher's note Springer Nature remains neutral with regard to jurisdictional claims in published maps and institutional affiliations.

Open Access This article is licensed under a Creative Commons Attribution 4.0 International License, which permits use, sharing, adaptation, distribution and reproduction in any medium or format, as long as you give appropriate credit to the original author(s) and the source, provide a link to the Creative Commons licence, and indicate if changes were made. The images or other third party material in this article are included in the article's Creative Commons licence, unless indicated otherwise in a credit line to the material. If material is not included in the article's Creative Commons licence and your intended use is not permitted by statutory regulation or exceeds the permitted use, you will need to obtain permission directly from the copyright holder. To view a copy of this licence, visit http://creativecommons.org/licenses/by/4.0/.

© The Author(s) 2024

Electronic Supplementary Material

Spatial and Temporal Variation in Surface Nitrate and Phosphate in the Northern Gulf of Mexico over 35 years

Authors:

Acosta, Kailani G.[1 *], 61 Route 9W, Palisades NY 10964, kailani.acosta@columbia.edu,

ORCID: 0000-0002-5216-8206

Juhl, Andrew R.[1], ORCID: 0000-0002-1575-3756, andyjuhl@ldeo.columbia.edu

Subramaniam, Ajit[1], ORCID: 0000-0003-1316-5827, ajit@ldeo.columbia.edu

Duhamel, Solange[2], ORCID: 0000-0002-8435-4695, duhamel@arizona.edu

Affiliation:

[1] Lamont-Doherty Earth Observatory, Columbia University, Palisades, NY, USA 10964

[2] Department of Molecular and Cellular Biology, University of Arizona, Tucson, AZ, USA 85721

Corresponding author information:

Kailani Acosta, kailani.acosta@columbia.edu

Supplementary Tables

Table S1 NGoM surface nutrient data sources. Data were compiled from the Biological & Chemical Oceanography Data Management Office (BCO-DMO), National Oceanic and Atmospheric Administration National Centers for Environmental Information World Ocean Database (NOAA NCEI WOD), United States Geological Survey (USGS), and Gulf of Mexico Research Initiative Information and Data Cooperative (GRIIDC). Our data set included only surface (0 to 5 m collection depth) nutrient data in the NGoM (defined as coordinates -98˚, -79˚ to 22.5˚, 31˚; see Figure 1) from 1985 to 2019, with most data collected in summer months (see Figure S1)

Years	Source	Cruise	Location	Month	# of samples	Units	Properties
1955 - 2019	USGS Lee, 2004	USGS MAR monitoring station	St. Francisville, LA	Monthly, Year round	408	Acre/ft (flow), Ton (load)	Flow, TDN load, TDP load, Temp, NO3+NO2 load, PO4, NH4, Chl a, Pigments, SiO3, pH, DO, suspended sediment, metals, pesticides
1985 - 2012	Cardona et al., 2016	GM0212, GM0303, GM306, GM0311, GM0404, GM0503, GM0509, GM0604, GM0606, GM0609, GM0704, GM0708	Shelf, Offshore	Year round	619	µM	Latitude, Longitude, Temp, Sal, Depth, NO2+NO3, NH4, PO4, Si
1985	Rabalais & Smith, 2017	LAHS 1985	LAHS	July, September	299	µM	Latitude, Longitude, Temp, Sal, Bottom Depth, Depth, NO3+NO2, PO4, NH4, Chl a, Phaeo, SiO3, pH ,DO
1986	Rabalais & Smith, 2017	LAHS 1986	LAHS	July	215	µM	Latitude, Longitude, Temp, Sal, Bottom Depth, Depth, NO3+NO2, PO4, NH4, Chl a, Phaeo, SiO3, pH ,DO
1987	Rabalais & Smith, 2017	LAHS 1987	LAHS	July	203	µM	Latitude, Longitude, Temp, Sal, Bottom Depth, Depth,

							NO3+NO2, PO4, NH4, Chl a, Phaeo, SiO3, pH ,DO
1985, 1986	Science Applications International Corp., 2002	WSK3051, Altair MX-43	Western GoM	October, January	55	µM	Latitude, Longitude, Temp, Sal, Bottom Depth, Depth, NO3+NO2, PO4, Si
1989	Murphy, 2002	Gyre 89G15	Offshore	Novemb er	10	µM	Latitude, Longitude, Temp, Sal, Depth, NO3+NO2, PO4, NH4, Si
1990	Rabalais, 2002	NECOP-90	Shelf	July, August	95	µM	Latitude, Longitude, Temp, Sal, DO, Depth, NO3+NO2, PO4, NH4, SiO3
1990	Rabalais & Smith, 2017	LATEX shelf	Shelf	July	3	µM	Latitude, Longitude, Temp, Sal, Bottom Depth, Depth, NO3+NO2, PO4, NH4, Chl a, Phaeo, SiO3
1991	Webb, 2002	Gyre WYU8126	Offshore	June	11	µM	Latitude, Longitude, Temp, Sal, Depth, NO3, PO4, Silicate
1991	Rabalais, 2002	NECOP-91	Shelf	Year round	28	µM	Latitude, Longitude, Temp, Sal, Depth, NO3+NO2, PO4, NH4, Chl a, Phaeo, SiO3, suspended sediments
1992	Rabalais, 2002	NECOP 92	Shelf	Year round	142	µM	Latitude, Longitude, Temp, Sal, Depth, NO3+NO2, PO4, NH4, Chl a, Phaeo, SiO3, suspended sediments
1992	Rabalais, 2002	NECOP 92	Shelf	April	132	µM	Latitude, Longitude, Temp, Sal, DO, Depth, NO3+NO2, PO4, NH4, Chl a, pH, SiO4
1993, 1994	Pittman, 2002	LATEX - A	Shelf	April - May	676	µmol/ L	Latitude, Longitude, Sal, Depth, DO, NO3+NO2, PO4, NH4, SiO3, chl a, urea, TSS
1993	Rabalais, 2002	NECOP 4-1993/ 7-1994	Shelf	April, July	825	µM	Latitude, Longitude, Temp, Sal, Depth, DO, NO3+NO2, PO4, NH4, chl a, phaeo, SiO3, suspended sediments
1994	Rabalais et al., 2017	LAHS 1994	LAHS	July	73	µM	Latitude, Longitude, Temp, Sal, Depth, NO3+NO2, PO4, NH4, SiO3
1994 - 2010	Parsons et al., 2014	-	Shelf	Year round	34	µM	Latitude, Longitude, Temp, Sal, Depth, NO2+NO3, NH4, PO4, SiO3, Chla, cell counts
1995	Rabalais & Smith, 2017	LAHS 1995	LAHS	July	74	µM	Latitude, Longitude, Temp, Sal, Depth, NO3+NO2, PO4, NH4, SiO3

1996	Rabalais & Smith, 2017	LAHS 1996	LAHS	July	76	µM	Latitude, Longitude, Temp, Sal, DO, Depth, NO3+NO2, PO4, NH4, SiO3
1997 - 2000	Howard, 2002	NEGOM 1 – 9 Gyre	Shelf	November, May - August	1191	µM, mg/m^3	Latitude, Longitude, Temp, Sal, Bottom Depth, Depth, DO, NO3+NO2, PO4, NH4, SiO3, Chl a, pigments
1997	Rabalais & Smith, 2017	LAHS 1997	LAHS	July	81	µM	Latitude, Longitude, Temp, Sal, DO, Depth, NO3+NO2, PO4, NH4, SiO3
1998	Rabalais & Smith, 2017	LAHS 1998	LAHS	year round	190	µM	Latitude, Longitude, Temp, Sal, Depth, NO3+NO2, PO4, NH4, SiO3
1999	Rabalais & Smith, 2017	LAHS 1999	LAHS	July	188	µM	Latitude, Longitude, Temp, Sal, Depth, NO3+NO2, PO4, NH4, SiO3
2000	Rabalais & Smith, 2017	LAHS 2000	LAHS	Year round	75	µM	Latitude, Longitude, Temp, Sal, Depth, NO3+NO2, PO4, NH4, SiO3
2000-2002	Rowe et al., 2002	NOCD 2192	Continental slope	May - June	107	µM, mg/m^3	Latitude, Longitude, Temp, Sal, Bottom Depth, Depth, DO, NO3+NO2, PO4, NH4, SiO3, urea, POC, PON, pigments
2001	Rabalais & Smith, 2017	LAHS 2001	LAHS	Year round	101	µM	Latitude, Longitude, Temp, Sal, Depth, NO3+NO2, PO4, NH4, SiO3
2002	Rabalais & Smith, 2017	LAHS 2002	LAHS	Year round	490	µM	Latitude, Longitude, Temp, Sal, Depth, NO3+NO2, PO4, NH4, SiO3
2003	Rabalais & Smith, 2017	LAHS 2003	LAHS	Year round	223	µM	Latitude, Longitude, Temp, Sal, Depth, DO, NO3+NO2, PO4, NH4, SiO3
2004	Rabalais & Smith, 2017	LAHS 2004	LAHS	Year round	240	µM	Latitude, Longitude, Temp, Sal, Depth, DO, NO3+NO2, PO4, NH4, SiO3
2004	Cardona et al., 2016	LC0401, LC0402, LC0403	Shelf	January - March	95	µM	Latitude, Longitude, Temp, Sal, Depth, NO3+NO2, PO4, NH4, chl a
2004	Cardona et al., 2016	SEAMAP	Shelf	May, June	99	µM	Latitude, Longitude, Temp, Sal, Bottom Depth, Depth, NO3+NO2, PO4, NH4, chl a
2004	Cardona et al., 2016	GM0503 GM0404	Shelf	May, June	98	µM	Latitude, Longitude, Temp, Sal, Bottom Depth, Depth, NO3+NO2, PO4, NH4, chl a

2005	Rabalais & Smith, 2017	LAHS 2005	LAHS	Year round	259	µM	Latitude, Longitude, Temp, Sal, Depth, NO3+NO2, SiO3, PO4, NH4
2006	Rabalais & Smith, 2017	LAHS 2006	LAHS	Year round	164	µM	Latitude, Longitude, Temp, Sal, Depth, NO3+NO2, SiO3, PO4, NH4
2007	Rabalais & Smith, 2017	LAHS 2007	LAHS	Year round	232	µM	Latitude, Longitude, Temp, Sal, Depth, NO3+NO2, SiO3, PO4, NH4, Chl a
2007	Langdon, 2010	GOMECC 2007	Shelf, offshore	July, August	95	µmol/ kg	Latitude, Longitude, Temp, Sal, Bottom Depth, Depth, DO, NO3+NO2, SiO3, PO4, NH4, Chl a, Silicate, CFCs, TOC, POC, DOC
2008	Cardona et al., 2016	MAGMIX	LAHS	May, November	99	µM	Latitude, Longitude, Temp, Sal, Bottom Depth, Depth, NO3+NO2, PO4, NH4, chl a
2008	Rabalais & Smith, 2017	LAHS 2008	LAHS	Year round	206	µM	Latitude, Longitude, Temp, Sal, Bottom Depth, Depth, NO3+NO2, PO4, NH4, SiO3
2009	Rabalais & Smith, 2017	LAHS 2009	LAHS	Year round	208	µM	Latitude, Longitude, Temp, Sal, Bottom Depth, Depth, NO3+NO2, PO4, NH4, SiO3
2010	Rabalais & Smith, 2017	LAHS 2010	LAHS	Year round	213	µM	Latitude, Longitude, Temp, Sal, Bottom Depth, Depth, NO3+NO2, PO4, NH4, SiO4, Chl a
2010	Montoya, 2016	OC468, EN496	Shelf, offshore	August - September	85	µM	Latitude, Longitude, Temp, Sal, Density, Depth, NO3+NO2, PO4, DO, N*
2010 - 2011	Shiller, 2014	R/V Pelican 2010	Deepwater Horizon area	May, October	29	µM	Latitude, Longitude, Temp, Sal, Depth, Bottom Depth, NO3+NO2, TDN, PO4, NH4, SiO4, O2, Chl a, Cs, Mo, Ra, Ba, V, Cr, Fe, Ni, Cu, Mn, Co, PAHs
2010 - 2013	Joye, 2016	EN510, EN515, EN528, FK006b, WS1010	GC600, Taylor Energy area	May - December	26	µM	Latitude, Longitude, Temp, Sal, Depth, NH4, NO3+NO2, TDN, TDP, DOC, DON, DOP, PO4, DO, pH, cell counts,
2010, 2011	Cardona et al., 2016	GOMEX2011, EN496, CH0711	Shelf, offshore	July	976	µM	Latitude, Longitude, Temp, Sal, Depth, DO, CDOM, NO2+NO3,

							NH4, PO4, SiO2, Chl a, cell counts
2011	Rabalais & Smith, 2017	LAHS 2011	LAHS	April - September	171	µM	Latitude, Longitude, Temp, Sal, Bottom Depth, Depth, NO3+NO2, PO4, NH4, SiO3
2011 - 2012	Daly, 2014	BE0412, WB0111, WB0211, WB0212, WB0511, WB0512, WB0611, WB0911, WB1111, WB1210	West Florida Shelf	January - November	761	µM	Temp, Depth, Urea, NO2+NO3, NH4, PO4, TDN, TDP, Si
2011, 2015, 2017, 2018	Howe et al., 2020	PE18-23, PE17-24, WBII 03 2015, WS1114	Offshore	April, June, November	8	µM	Latitude, Longitude, Sal, Depth, NO3+NO2, d18O
2012	Rabalais, 2017	LAHS 2012	LAHS	May - September	136	µM	Latitude, Longitude, Temp, Sal, Bottom Depth, Depth, NO3+NO2, PO4, NH4, SiO4
2012	Kostka et al., 2014	WB-1306CT7	Seeps (Peanut Seep, A, B, C)	September - October	4	µM	Latitude, Longitude, Temp, Sal, Depth, PP, NO2+NO3, NH4, PO4, SiOH4, DO, Turbidity, Density, Chl a, CH4
2012	Montoya, 2019	EN509	Shelf, Offshore	May-June	38	µM	Latitude, Longitude, Temp, Sal, Density, Depth, NO3+NO2, PO4, DO, N*
2012	Stewart et al., 2015	CH0212	Shelf	July - August	64	µM	Latitude, Longitude, Depth, Temp, Sal, NO3+NO2
2012 - 2013	Sutor, 2015	Walton Smith	Offshore	April	895	µM	Latitude, Longitude, Depth, Temp, Sal, Density, NH4, N+N, NO2
2012 - 2014	Daly, 2015	R/V Bellows	West Florida Shelf	April - November	930	µM	Temp, Depth, Urea, NO2+NO3, NH4, PO4, TDN, TDP, Si
2013	Montoya, 2016	R/V Arcadiana, R/V Weatherbird	NGoM Hercules Spill Response	July - August	9	µM	Latitude, Longitude, Sal, Density, Depth, NH4, NO3+NO2, TDN, TDP, DOC, DON, DOP, PO4, DO, pH, cell counts
2013	Rabalais & Smith, 2017	LAHS 2013	LAHS	July	89	µM	Latitude, Longitude, Temp, Sal, Bottom Depth, Depth, NO3+NO2, PO4, NH4, SiO4
2014	Roberts, 2016	R/V Pelican PE-15-01 LUMCON	Plume to offshore NGoM	July	82	µM	Latitude, Longitude, Temp, Depth, PP, NO2+NO3, NH4, PO4, SiO2, DO, Chl a, Phaeo

2014	Rabalais, 2017	LAHS 2014	LAHS	July	178	µM	Latitude, Longitude, Temp, Sal, Bottom Depth, Depth, NO3+NO2, PO4, NH4, SiO3
2015	Barbero et al., 2016	WS1509	OAP 2015	September	30	µmol/kg	Latitude, Longitude, Temp, Sal, Bottom Depth, Depth, NO3+NO2, PO4, DIC, Silicate, pH
2015, 2016	Krause & Acton, 2018	PTS01	Shelf	October, November	48	ug/L	Latitude, Longitude, Depth, Bottom Depth, POC, PON, Chl a
2015	Shiller, 2017	R/V Pt. Sur CONCORDE BCS 2015, 2016	Mississippi Bight	October, November,February, July	102	umol/kg	Latitude, Longitude, Temp, Sal, Depth, NO3+NO2, PO4, NH4, SiO4, O2, Chl a
2015, 2016	Joye, 2018; Zhuang et al., 2018	EN559, EN586		May - June	10	µmol/L	Latitude, Longitude, Sal, Depth, NO3, NH4, PO4, DOC, Chl a
2016	Caffrey, 2017		Pensacola shelf	July	73	TN (ug N/L) Si (mg/L) TKN/TP (mg N/ mg P)	Total Nitrate/Nitrite, Total Kjeldahl Nitrogen (FIA), Total Phosphorus (FIA), Silica
2016	Rabalais, 2019	LAHS 2016	LAHS	August	21	µM	Latitude, Longitude, Temp, Sal, Bottom Depth, Depth, NO3+NO2, PO4, NH4, SiO3
2016	Joye, 2019	EN586	NGoM	July - August	310	µM	Latitude, Longitude, Sal, Depth, NH4, NO3+NO2, TDN, TDP, DOC, DON, DOP, PO4, DO
2016, 2017	Krause et al., 2019	CLASiC2016, CLASiC2017	Shelf	May, August, September	59	µM	Latitude, Longitude, Temp, Sal, Oxygen, Depth, Bottom Depth, NO3, NO2, NH4, PO4, Silicate, pheophytin, Chl a,
2017	Rabalais, 2020	LAHS 2017	LAHS	July	93	µM	Latitude, Longitude, Temp, Sal, Bottom Depth, Depth, NO3+NO2, PO4, NH4, SiO4
2017	Olascoaga, M.J., 2019	GOMECC3	Shelf, Offshore	July, August	1631	µmol/kg	Latitude, Longitude, Temp, Sal, Bottom Depth, Depth, DO, NO3+NO2, SiO3, PO4, NH4, Chl a, Silicate, CFCs, TOC, POC, DOC

2017	Kamalanatha n et al., 2019	PS1809	Shelf	Septemb er, October	126	µmol/ L, ug/L	Latitude, Longitude, Temp, Sal, Depth, Bottom Depth, NO3, NO2, NH4, PO4, Urea
2018	Rabalais, 2020	LAHS 2018	LAHS	July	51	µM	Latitude, Longitude, Temp, Sal, Bottom Depth, Depth, DO, NO3+NO2, PO4, NH4, SiO4
2018, 2019	This Study	EN620, EN642	Offshore, shelf	July, August	89	µM	Latitude, Longitude, Sal, Density, Depth, NO3+NO2, PC, PN, PP, TDN, TDP, DON, DOP, PO4, DO, cell counts, pigments
2019	Barbero et al., 2019	WS19119, WS19210,WS19 266	OAP 19	May - October	20	µmol/ kg	Latitude, Longitude, Temp, Sal, Bottom Depth, Depth, NO3+NO2, PO4, DIC, Silicate, pH

References

Barbero, L.,Wanninkhof, R., & Pierrot, D. (2016). Dissolved inorganic carbon, total alkalinity, pH, nutrients, and other variables collected from surface discrete observations using Niskin bottle and other instruments from R/V F. G. Walton Smith in the west coast of Florida within Gulf of Mexico from 2015-09-21 to 2015-09-25 (NCEI Accession 0157025). NOAA National Centers for Environmental Information. Dataset. https://doi.org/10.7289/v5ws8r98.

Barbero, L.,Wanninkhof, R., & Pierrot, D. (2019). Dissolved inorganic carbon, total alkalinity, pH, nutrients, and other variables collected from surface discrete observations using Niskin bottle and other instruments during the R/V F. G. Walton Smith cruise WS19028 (EXPOCODE 33WA20190128) in the west coast of Florida, Gulf of Mexico from 2019-01-28 to 2019-02-01 (NCEI Accession 0188977). [indicate subset used]. NOAA National Centers for Environmental Information. Dataset. https://doi.org/10.25921/dnxy-k985.

Caffrey, J. (2017). Surface and Bottom Water Nutrient Data July 2016, Pensacola Shelf. Distributed by: Gulf of Mexico Research Initiative Information and Data Cooperative (GRIIDC), Harte Research Institute, Texas A&M University–Corpus Christi. doi:10.7266/N7DZ06QP

Cardona, Y., Bracco, A., Villareal, T. A., Subramaniam, A., Weber, S. C., & Montoya, J. P. (2016). Highly variable nutrient concentrations in the Northern Gulf of Mexico. *Deep-Sea Research Part II: Topical Studies in Oceanography*, *129*, 20–30. https://doi.org/10.1016/j.dsr2.2016.04.010

Daly, K. (2014). Nutrient concentrations for the northeastern Gulf of Mexico and west Florida shelf, July 2010 – May 2012.. Distributed by: Gulf of Mexico Research Initiative Information and Data Cooperative (GRIIDC), Harte Research Institute, Texas A&M University–Corpus Christi. doi:10.7266/N7R78C41

Daly, K. (2015). Nutrient concentrations for the northeastern Gulf of Mexico and west Florida shelf: June 2012 – August 2014. Distributed by: Gulf of Mexico Research Initiative Information and Data Cooperative (GRIIDC), Harte Research Institute, Texas A&M University–Corpus Christi. doi:10.7266/N7G73BMH

Howard, M. K. (2002). Chemical, current meter, and other data from current meter, bottle, XBT, and CTD casts in the Gulf of Mexico as part of the Northeastern Gulf of Mexico Physical Oceanographic Program: Chemical Oceanography and Hydrography Study (NEGOM) project, 1997-11-16 to 2000-08-08 (NCEI Accession 0000703). NOAA National Centers for Environmental Information. https://www.ncei.noaa.gov/archive/accession/0000703.

Joye, S. (2016). Water column 16S rRNA libraries, geochemical data, and process rate data collected from the Northern Gulf of Mexico before, during, and after the Deepwater Horizon Event March 2010 - November 2012. Distributed by: Gulf of Mexico Research Initiative Information and Data Cooperative (GRIIDC), Harte Research Institute, Texas A&M University–Corpus Christi. doi:10.7266/N7DV1GWK

Joye, S. (2018). Methanol and methylamine oxidation rate measurements, geochemistry, and bacterial production in the northern Gulf of Mexico water column, May 2015 to August 2016. Distributed by: Gulf of Mexico Research Initiative Information and Data Cooperative (GRIIDC), Harte Research Institute, Texas A&M University–Corpus Christi. doi:10.7266/N7SF2TPP

Joye, S. (2019). Geochemical data collected from R/V Endeavor cruise EN585 at the Orca Basin in the Gulf of Mexico on 2016-07-29. Distributed by: Gulf of Mexico Research Initiative Information and Data Cooperative (GRIIDC), Harte Research Institute, Texas A&M University–Corpus Christi. doi:10.7266/n7-3bp5-sb94

Kamalanathan, M., Mapes, S., Hillhouse, J., Claflin, N., Campbell, D., & Quigg, A. (2019). How does oil exposure affect centric diatom Thalassiosira pseudonana?. Distributed by: Gulf of Mexico Research Initiative Information and Data Cooperative (GRIIDC), Harte Research Institute, Texas A&M University–Corpus Christi. doi:10.7266/BSYXMGD0

Kostka J. E., Teske AP, Joye S. B., Head I.M. (2014). The metabolic pathways and environmental controls of hydrocarbon biodegradation in marine ecosystems. *Frontiers in Microbiology* (*5*)471. doi: 10.3389/fmicb.2014.00471.

Krause, J.W. & Acton, S. (2018). Size-fractionated nitrate uptake and primary productivity on the Mississippi-Alabama Shelf, March to July, 2016. Distributed by: Gulf of Mexico Research Initiative Information and Data Cooperative (GRIIDC), Harte Research Institute, Texas A&M University–Corpus Christi. doi:10.7266/N74B2ZVN

Krause, J.W., Thamatrakoln, K., Cole, L., & Acton, S. (2019). Seasonal effects on microplankton response to oil perturbation on Mississippi-Alabama shelf, Gulf of Mexico from 2016-01-24 to 2017-03-16. Distributed by: Gulf of Mexico Research Initiative Information and Data Cooperative (GRIIDC), Harte Research Institute, Texas A&M University–Corpus Christi. doi:10.7266/n7-w8zg-tj49

Langdon, C. (2010). Temperature, salinity, nutrients, freons, oxygen, currents (ADCP), underway and other measurements collected in the Gulf of Mexico and Atlantic as part of the Gulf of Mexico and East Coast Carbon Cruise (GOMECC) 2007 (NCEI Accession 0066603). NOAA National Centers for Environmental Information. Dataset. https://www.ncei.noaa.gov/archive/accession/0066603.

Lee, C. (2022). Nutrient loads to the Gulf of Mexico produced by the USGS National Water Quality Network, 1968-2021: U.S. Geological Survey, https://doi.org/10.5066/P9G0EEUE

Montoya, J. (2016). Hercules Spill Response Cruises, Water Chemistry. Louisiana South Timbalier Block 220, 27-30 July (R/V Acadiana) and 25 August (R/V Weatherbird) 2013. Distributed by: Gulf of Mexico Research Initiative Information and Data Cooperative (GRIIDC), Harte Research Institute, Texas A&M University–Corpus Christi. doi:10.7266/N7125QNH

Montoya, J. (2016). Particle and zooplankton sample elemental (C, N) and isotopic (13C, 15N) data from Cruise OC468, EN496, Louisiana, Mississippi, Alabama Self Break, August and September, 2010. Distributed by: Gulf of Mexico Research Initiative Information and Data Cooperative (GRIIDC), Harte Research Institute, Texas A&M University–Corpus Christi. doi:10.7266/N7X06521

Montoya, J. (2019). Particle and zooplankton sample elemental (C,N) and isotopic (13C, 15N) data, Cruise EN509, northern Gulf of Mexico, May 26 - June 19, 2012. Distributed by: Gulf of Mexico Research Initiative

Information and Data Cooperative (GRIIDC), Harte Research Institute, Texas A&M University–Corpus Christi. doi:10.7266/N7NK3C2R

Murphy, D. (2002). Cloud amount/frequency, NITRATE and other data from GYRE in the Gulf of Mexico from 1989-11-11 to 1989-11-18 (NCEI Accession 9000025). NOAA National Centers for Environmental Information. https://www.ncei.noaa.gov/archive/accession/9000025.

Olascoaga, M.J. (2019). Drifters released during the Gulf of Mexico Ecosystems and Carbon Cycle (GOMECC-3) cruise in the Gulf of Mexico from 2017-07-22 to 2017-09-17. Distributed by: Gulf of Mexico Research Initiative Information and Data Cooperative (GRIIDC), Harte Research Institute, Texas A&M University–Corpus Christi. doi:10.7266/N7G44NW5

Ozhan, K., Parsons, M. L., & Bargu, S. (2014). How Were Phytoplankton Affected by the Deepwater Horizon Oil Spill? *BioScience*, *64*(9), 829–836. https://doi.org/10.1093/BIOSCI/BIU117

Pittman, R.V. (2002). BAROMETRIC PRESSURE and Other Data from GYRE From Gulf of Mexico from 1993-10-28 to 1993-11-03 (NCEI Accession 9400017). NOAA National Centers for Environmental Information. Dataset. https://www.ncei.noaa.gov/archive/accession/9400017.

Rabalais, N. N. (2002). Chemical, zooplankton, and phytoplankton data from CTD and other instruments in the Mississippi River and Gulf of Mexico as part of the Nutrient Enhanced Coastal Ocean Productivity (NECOP) project, from 1985-07-15 to 1993-05-12 (NCEI Accession 9800129). NOAA National Centers for Environmental Information. Dataset. https://www.ncei.noaa.gov/archive/accession/9800129.

Rabalais, N. N. (2017). Physical (Hydrography), chemical (CTD), and biological (Water Quality) processes of the Texas-Louisiana continental shelf, 2012 (NCEI Accession 0162101). NOAA National Centers for Environmental Information. Dataset. https://www.ncei.noaa.gov/archive/accession/0162101.

Rabalais, N. N. (2017). Physical (Hydrography), chemical (CTD), and biological (Water Quality) processes of the Texas-Louisiana continental shelf, 2014 (NCEI Accession 0161219). NOAA National Centers for Environmental Information. Dataset. https://www.ncei.noaa.gov/archive/accession/0161219.

Rabalais, N. N. (2019). Water temperature, salinity, and other physical, chemical, and biological parameters taken by CTD and multi parameter water quality sonde on board of research vessel Pelican on the Texas-Louisiana continental shelf, Gulf of Mexico from 2016-06-14 2016-10-26 (NCEI Accession 0205845). NOAA National Centers for Environmental Information. Dataset. https://doi.org/10.25921/5903-cp08.

Rabalais, N. N. (2020). Physical (hydrography), chemical (CTD), and biological (water quality) processes of the Texas-Louisiana continental shelf, 2017 (NCEI Accession 0208325). NOAA National Centers for Environmental Information. Dataset. https://www.ncei.noaa.gov/archive/accession/0208325.

Rabalais, N. N. (2020). Physical (hydrography), chemical (CTD), and biological (water quality) processes of the Texas-Louisiana continental shelf, 2018 (NCEI Accession 0219157). NOAA National Centers for Environmental Information. Dataset. https://www.ncei.noaa.gov/archive/accession/0219157.

Rabalais, N. N., & Smith, L. (2017). Bottom-water area of Louisiana-Texas continental shelf hypoxia 1985-2014. Distributed by: Gulf of Mexico Research Initiative Information and Data Cooperative (GRIIDC), Harte Research Institute, Texas A&M University–Corpus Christi. doi:10.7266/N7GF0RKZ

Rabalais, N. N., Turner, R. E., & Wiseman, W. J.., Jr. (2017). Hydrographic and chemical water parameters collected by CTD and other instruments from the Pelican and the Tommy Munro in coastal waters of Louisiana from 1994-07-24 to 1997-07-29 (NCEI Accession 0164298). NOAA National Centers for Environmental Information. Dataset. https://www.ncei.noaa.gov/archive/accession/0164298.

Roberts, B. (2016). Dissolved inorganic nutrients, pigments, and dissolved oxygen concentrations collected during R/V Pelican cruise July 7-10 2014, northern Gulf of Mexico near DeSoto Canyon, PE15-01. Distributed by: Gulf of Mexico Research Initiative Information and Data Cooperative (GRIIDC), Harte Research Institute, Texas A&M University–Corpus Christi. doi:10.7266/N7BZ63Z7

Rowe, G. T., Cruz Kaegi, M.E., Morse, J. W., Boland, G. S., & Escobar Briones, E.G. (2002). Sediment Community Metabolism Associated with Continental Shelf Hypoxia, Northern Gulf of Mexico. *Estuaries*, *25*(6), 1097–1106. http://www.jstor.org/stable/1353154

Science Applications International Corporation. (2002). Current meter data from moored current meter casts in the Gulf of Mexico as part of the Gulf of Mexico Physical Oceanography (GMPO) project, from 1983-01-26 to 1985-01-01 (NCEI Accession 8600064). NOAA National Centers for Environmental Information. Dataset. https://www.ncei.noaa.gov/archive/accession/8600064.

Shiller, A.M. (2014). Dissolved trace metal and ancillary data (including nutrients and dissolved oxygen) in the vicinity of the Deepwater Horizon blowout, May 2010-October 2011.. Distributed by: Gulf of Mexico Research Initiative Information and Data Cooperative (GRIIDC), Harte Research Institute, Texas A&M University–Corpus Christi. doi:10.7266/N7MS3QQ5

Shiller, A.M. (2017). Geochemical CTD/rosette data for cruise PTS01 in the Mississippi Bight, Fall 2015. Distributed by: Gulf of Mexico Research Initiative Information and Data Cooperative (GRIIDC), Harte Research Institute, Texas A&M University–Corpus Christi. doi:10.7266/N7F769NC

Stewart, P. S., Feng, J., Kimptom, L. S., Griffiths, I.M., & Stone, H.A. (2015). Dataset supporting the publication "Stability of a bi-layer free film: simultaneous or individual rupture events?". Distributed by: Gulf of Mexico Research Initiative Information and Data Cooperative (GRIIDC), Harte Research Institute, Texas A&M University–Corpus Christi. doi:10.7266/N79Z92V9

Sutor, M. (2015). Inorganic nutrients in Gulf of Mexico, spring 2012 and spring 2013. Distributed by: Gulf of Mexico Research Initiative Information and Data Cooperative (GRIIDC), Harte Research Institute, Texas A&M University–Corpus Christi. doi:10.7266/N77S7KQM

van Hooidonk, R. (2022). Modeled ocean acidification data in the Gulf of Mexico and wider Caribbean using satellites and climate model data for the Ocean Acidification Products for the Gulf of Mexico and East Coast project from 2014-01-01 to 2020-12-31 (NCEI Accession 0245950). NOAA National Centers for Environmental Information. Dataset. https://doi.org/10.25921/tt1c-dx53.

Webb, E. (2002). Cloud amount/frequency, NITRATE and other data from GYRE in the Gulf of Mexico from 1991-03-02 to 1991-03-09 (NCEI Accession 9100092). NOAA National Centers for Environmental Information. Dataset. https://www.ncei.noaa.gov/archive/accession/9100092.

Zhuang, G. C., Montgomery, A., Sibert, R. J., Rogener, M. K., Samarkin, V. A., & Joye, S. B. (2018). Effects of pressure, methane concentration, sulfate reduction activity, and temperature on methane production in surface sediments of the Gulf of Mexico. *Limnology and Oceanography*, *63*(5), 2080–2092. https://doi.org/10.1002/LNO.10925

Table S2 Summary statistics for annual mean N and P loading from the MAR into the NGoM. The corresponding plots are shown in Figure 3. Linear regression equations, r^2, *p* values, and *n* for mean annual N and P loading into the NGoM from 1985 to 2019. Significant regressions are shaded green. Based on USGS data (Lee, 2022)

N	**Regression Equation**	r^2	***p* value**	***n***	**P**	**Regression Equation**	r^2	***p* value**	***n***
TN	$y = 1.6 \times 10^9 - 2.8 \times 10^6 x$	-0.08	0.65	34	TP	$y = 1.4 \times 10^8 + 1.6 \times 10^6 x$	0.44	0.009	34
DIN	$y = 9.7 \times 10^8 + 3.4 \times 10^6 x$	0.05	0.74	34	DIP	$y = 3.6 \times 10^7 + 7.6 \times 10^5 x$	0.48	0.004	34
DON	$y = 6.4 \times 10^8 - 6.2 \times 10^6 x$	-0.43	0.01	34	DOP	$y = 1.0 \times 10^8 + 8.8 \times 10^5 x$	0.31	0.05	34

Table S3 Regression results to test for temporal trends in mean annual nutrient concentrations (DIN, DIP, and DIN:DIP) for each regional subset of the NGoM from 1985 to 2019; hypoxic region, shelf region, offshore region (see Figure S5). Entire data set annual mean nutrient concentrations are shown in Figure 2

Region	Nutrient (µM)	Regression Equation	r^2	*p* value	*n*
Hypoxic	[DIN]	y = 5.2 – 0.06x	0.04	0.30	32
Hypoxic	[DIP]	y = 0.3 + 0.01x	0.19	0.012	31
Hypoxic	DIN:DIP	y = 10 – 0.15x	0.04	0.24	32
Shelf	[DIN]	y = 4.8 – 0.04x	0.02	0.45	32
Shelf	[DIP]	y = 0.33 + 0.01x	0.16	0.023	31
Shelf	DIN:DIP	y = 9.7 – 0.14x	0.04	0.27	32
Offshore	[DIN]	y = 4.5 – 0.08x	0.02	0.52	32
Offshore	[DIP]	y = 0.13 – 0.003x	0.03	0.43	32
Offshore	DIN:DIP	y = 4.4 + 0.01x	0.11	0.87	32

Table S4 Correlation tables for annual mean MAR nutrient concentrations, discharge, and loading vs. NGoM annual mean nutrient concentrations. Annual mean nutrient concentrations are calculated using data from St. Francisville, LA, and discharge values are from the MAR combined flow into the NGoM in m^3 (Figure S3). Pearson correlation coefficients (r) and p values shown for the entire NGoM dataset, and each of three regional subsets of the data. Significant p-values < 0.05 are shaded green. Because of excluded NGoM data in 1988 and 2014, n = 32 for all correlations. Based on USGS data (Lee, 2022)

Region	Annual Mean Nutrient	MAR discharge	MAR DIN load	MAR [DIN]	MAR DIP load	MAR [DIP]	MAR DIN:DIP
Entire NGoM	NGoM DIN	r = 0.32 p = 0.04	r = 0.48 p = 0.002	r = 0.49 p = 0.001	r = 0.37 p = 0.02	r = 0.49 p = 0.001	r = 0.42 p = 0.01
Entire NGoM	NGoM DIP	r = 0.45 p = 0.003	r = 0.53 p = 0.004	r = 0.52 p = 0.001	r = 0.57 p < 0.001	r = 0.65 p < 0.001	r = 0.38 p = 0.02
Entire NGoM	NGoM DIN:DIP	r = 0.26 p = 0.10	r = 0.44 p = 0.004	r = 0.44 p = 0.005	r = 0.37 p = 0.02	r = 0.44 p = 0.004	r = 0.33 p = 0.04
Hypoxic Region	Hypoxic DIN	r = 0.32 p = 0.05	r = 0.50 p = 0.001	r = 0.49 p = 0.001	r = 0.36 p = 0.02	r = 0.49 p = 0.001	r = 0.45 p = 0.004
Hypoxic Region	Hypoxic DIP	r = 0.41 p = 0.01	r = 0.52 p = 0.001	r = 0.50 p = 0.001	r = 0.53 p < 0.001	r = 0.62 p < 0.001	r = 0.39 p = 0.02
Hypoxic Region	Hypoxic DIN:DIP	r = 0.27 p = 0.10	r = 0.44 p = 0.004	r = 0.43 p = 0.005	r = 0.35 p = 0.03	r = 0.43 p = 0.005	r = 0.34 p = 0.03
Shelf	Shelf DIN	r = 0.33 p = 0.04	r = 0.48 p = 0.002	r = 0.48 p = 0.002	r = 0.36 p = 0.02	r = 0.50 p = 0.001	r = 0.43 p = 0.01
Shelf	Shelf DIP	r = 0.43 p = 0.01	r = 0.52 p = 0.001	r = 0.50 p = 0.001	r = 0.55 p < 0.001	r = 0.63 p < 0.001	r = 0.38 p = 0.02
Shelf	Shelf DIN:DIP	r = 0.26 p = 0.10	r = 0.44 p = 0.005	r = 0.43 p = 0.006	r = 0.36 p = 0.02	r = 0.44 p = 0.005	r = 0.33 p = 0.04
Off shore	Offshore DIN	r = 0.12 p = 0.45	r = 0.12 p = 0.44	r = 0.09 p = 0.60	r = 0.05 p = 0.77	r = 0.06 p = 0.71	r = 0.19 p = 0.24
Off shore	Offshore DIP	r = 0.43 p = 0.01	r = 0.27 p = 0.09	r = 0.30 p = 0.06	r = 0.23 p = 0.15	r = 0.33 p = 0.04	r = 0.28 p = 0.01
Off shore	Offshore DIN:DIP	r = 0.41 p = 0.01	r = 0.36 p = 0.02	r = 0.36 p = 0.02	r = 0.36 p = 0.02	r = 0.41 p = 0.01	r = 0.25 p = 0.11

Table S5 Correlations of annual mean nutrient concentrations for NGoM shelf region vs. offshore region. Table shows Pearson correlation coefficients (r) and p values. Correlation analyses were not conducted separately for the hypoxic region because it is a subset of the shelf region and therefore included in the shelf data. Significant values are shaded green

Region	Shelf [DIN]	Shelf [DIP]	Shelf (DIN:DIP)
Offshore [DIN]	r = 0.07 p = 0.67	r = 0.13 p = 0.44	r = 0.05 p = 0.76
Offshore[DIP]	r = 0.28 p = 0.07	r = 0.24 p = 0.13	r = 0.04 p = 0.82
Offshore (DIN:DIP)	r = 0.32 p = 0.04	r = 0.36 p = 0.02	r = 0.04 p = 0.83

Table S6 Results of correlation analyses comparing annual area of hypoxic bottom water to mean annual NGoM surface nutrient concentrations. Pearson correlation coefficients (*r*) and *p* values presented for (a) MAR nutrient loading, (b) the entire NGoM, and for 3 NGoM subregions (c – e). The annual area of hypoxic bottom water is from Rabalais and Turner, (2019) and annual mean nutrient data are shown in Figures 3 and S4 with accompanying summary statistics listed in Table S5 (n = 32). Significant values < 0.05 are shaded green

Annual hypoxic area vs.	**Correlation Coefficient (Pearson's *r*)**	***p* value**
a MAR nutrient loading		
vs. mean annual DIN load	0.68	< 0.0001
vs. mean annual DON load	0.34	0.03
vs. mean annual TN load	0.59	< 0.0001
vs. mean annual DIP load	0.69	< 0.0001
vs. mean annual DOP load	0.41	0.01
vs. mean annual TP load	0.52	0.001
b Entire NGoM dataset		
vs. mean annual [DIN]	0.33	0.04
vs. mean annual [DIP]	0.33	0.04
vs. mean annual DIN:DIP	0.41	0.01
c Hypoxic region		
vs. mean annual [DIN]	0.34	0.03
vs. mean annual [DIP]	0.31	0.05
vs. mean annual DIN:DIP	0.41	0.01
d Shelf region		
vs. mean annual [DIN]	0.34	0.03
vs. mean annual [DIP]	0.31	0.05
vs. mean annual DIN:DIP	0.41	0.01
e Offshore region		
vs. mean annual [DIN]	-0.07	0.65
vs. mean annual [DIP]	-0.09	0.59
vs. mean annual DIN:DIP	0.21	0.20

Table S7 Regression results to test for salinity trends in NGoM surface nutrients by regional subset 1985–2019: (a) hypoxic ln[DIN]; (b) hypoxic ln[DIP]; (c) hypoxic ln(DIN:DIP); (d) shelf ln[DIN]; (e); shelf ln[DIP]; (f) shelf ln(DIN:DIP); (g) offshore ln[DIN]; (h) offshore ln[DIP]; (i) offshore ln(DIN:DIP) – NGoM nutrient concentrations vs. salinity for all regions combined are shown in Figure 4. The corresponding regional plots are shown in Figure S5a-i. Significant regressions are shaded green

	Region	**Nutrient (µM)**	**Regression Equation**	r^2	***p* value**	***n***
a	Hypoxic	ln[DIN]	y = -0.15x + ln(102.41)	0.25	< 0.0001	5671
b	Hypoxic	ln[DIP]	y = -0.07x + ln(2.19)	0.14	< 0.0001	5455
c	Hypoxic	ln(DIN:DIP)	y = -0.11x + ln(46.78)	0.001	0.02	5414
d	Shelf	ln[DIN]	y = -0.18x + ln(102.41)	0.26	< 0.0001	6313
e	Shelf	ln[DIP]	y = -0.07x + ln(2.19)	0.17	< 0.0001	6024
f	Shelf	ln(DIN:DIP)	y = -0.11x + ln(46.78)	0.001	0.01	5981
g	Offshore	ln[DIN]	y = -0.19x + ln(102.41)	0.34	< 0.0001	1428
h	Offshore	ln[DIP]	y = -0.10x + ln(2.19)	0.22	< 0.0001	1452
i	Offshore	ln(DIN:DIP)	y = -0.09x + ln(46.78)	0.03	< 0.0001	1392

Supplementary Figures

Figure S1

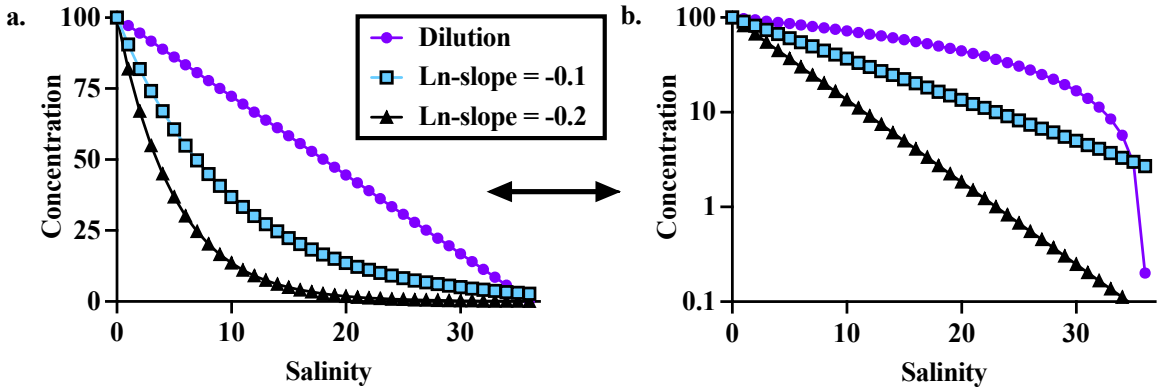

Fig. S1 Nutrient concentration vs. salinity plots for a hypothetical nutrient with a concentration at zero salinity of 100 (in arbitrary units). The same underlying data is plotted on both (a.) and (b.) though in (b.) the y-axis is log-scale (as in Fig. 4). The dilution-only mixing function (purple dots) is calculated by assuming that the nutrient declines in proportion to increasing salinity, resulting in a line in (a.) and a curve in (b.). The blue and black data points in both plots were calculated using the linear equations $\ln(y) = -0.1x + \ln(100)$, and $\ln(y) = -0.2x + \ln(100)$. These figures demonstrate that the linear mixing functions used in this study should appear curved on semi-log plots. In addition, the figures exemplify why an increasing slope of ln-transformed nutrient vs. salinity relationships primarily reflects higher relative loss of the nutrient at low salinities

Fig S2

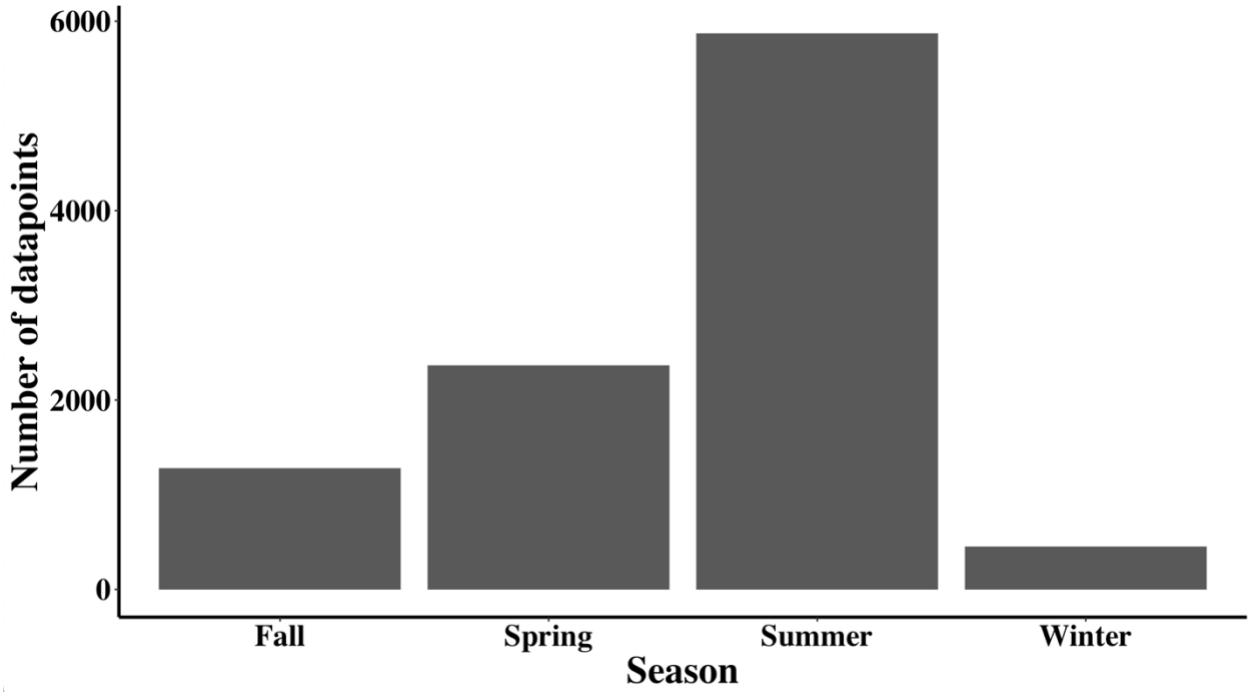

Fig. S2 Distribution of data points by season, based on collection date. Seasons are defined as Fall (September, October, November), Spring (March, April, May), Summer (June, July, August), and Winter (December, January, February). Each data point equates to an individual sample collected in a given year at a given location (latitude/longitude) and depth

Fig S3

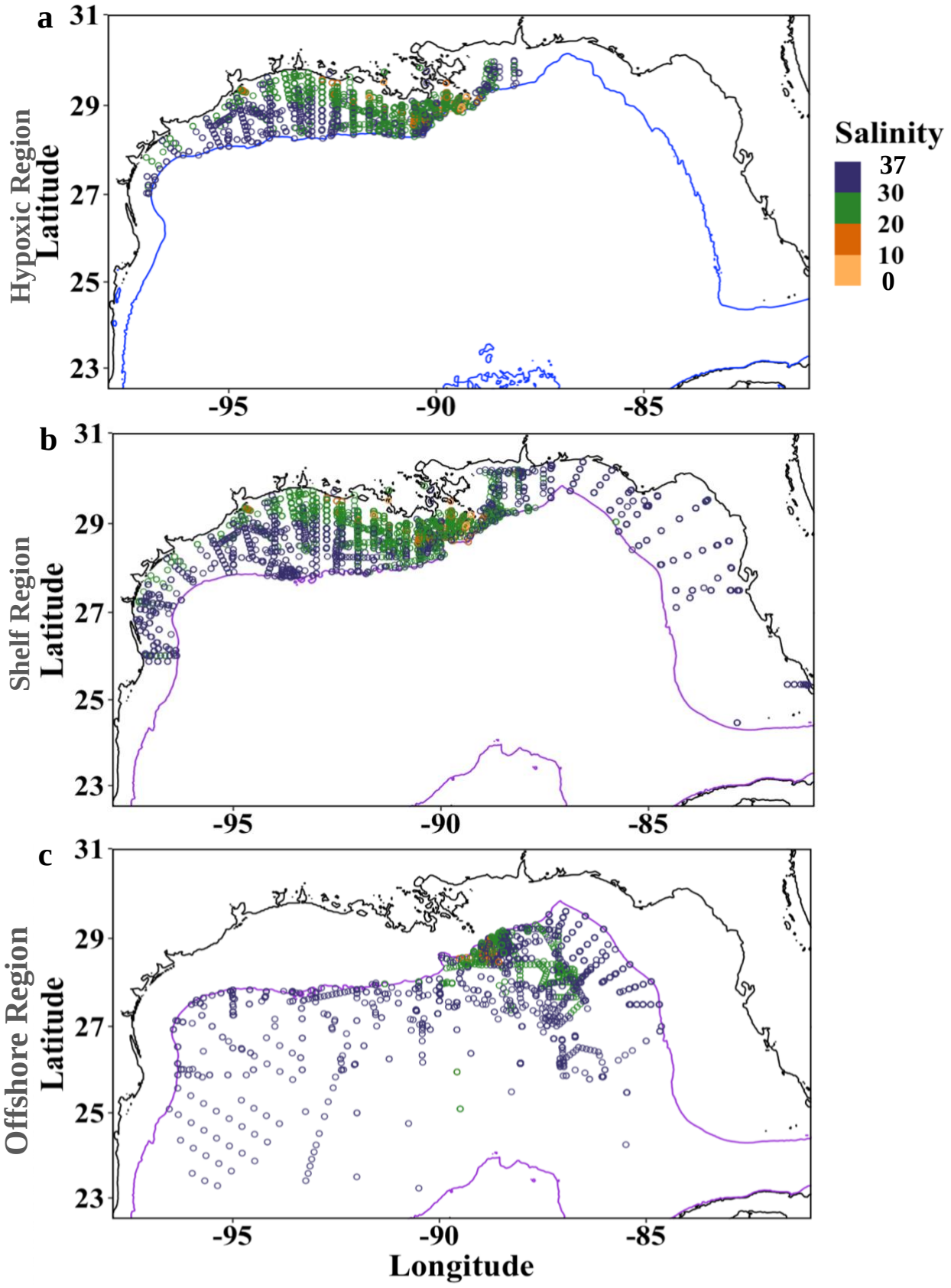
a
b
c
Hypoxic Region
Shelf Region
Offshore Region
Latitude
Longitude
31
29
27
25
23
-95
-90
-85
Salinity
37
30
20
10
0

Fig. S3 NGoM nutrient sampling stations 1985–2019 (excluding 1988 and 2014) for the (a) hypoxic, (b) shelf, and (c) offshore regions. Circles represent individual surface samples (0 - 5 meter collection depth). Circle color denotes sample salinity. Bathymetry isobaths denote the 60 meter (in a; blue line) and 200 meter (in b and c; purple line) depth isobaths. The hypoxic region is a subset of the shelf samples within longitudes -88° to -97° and latitudes 27° to 30° where bottom depths were < 60 meters (Rabalais & Turner, 2019; gulfhypoxia.net)

Figure S4

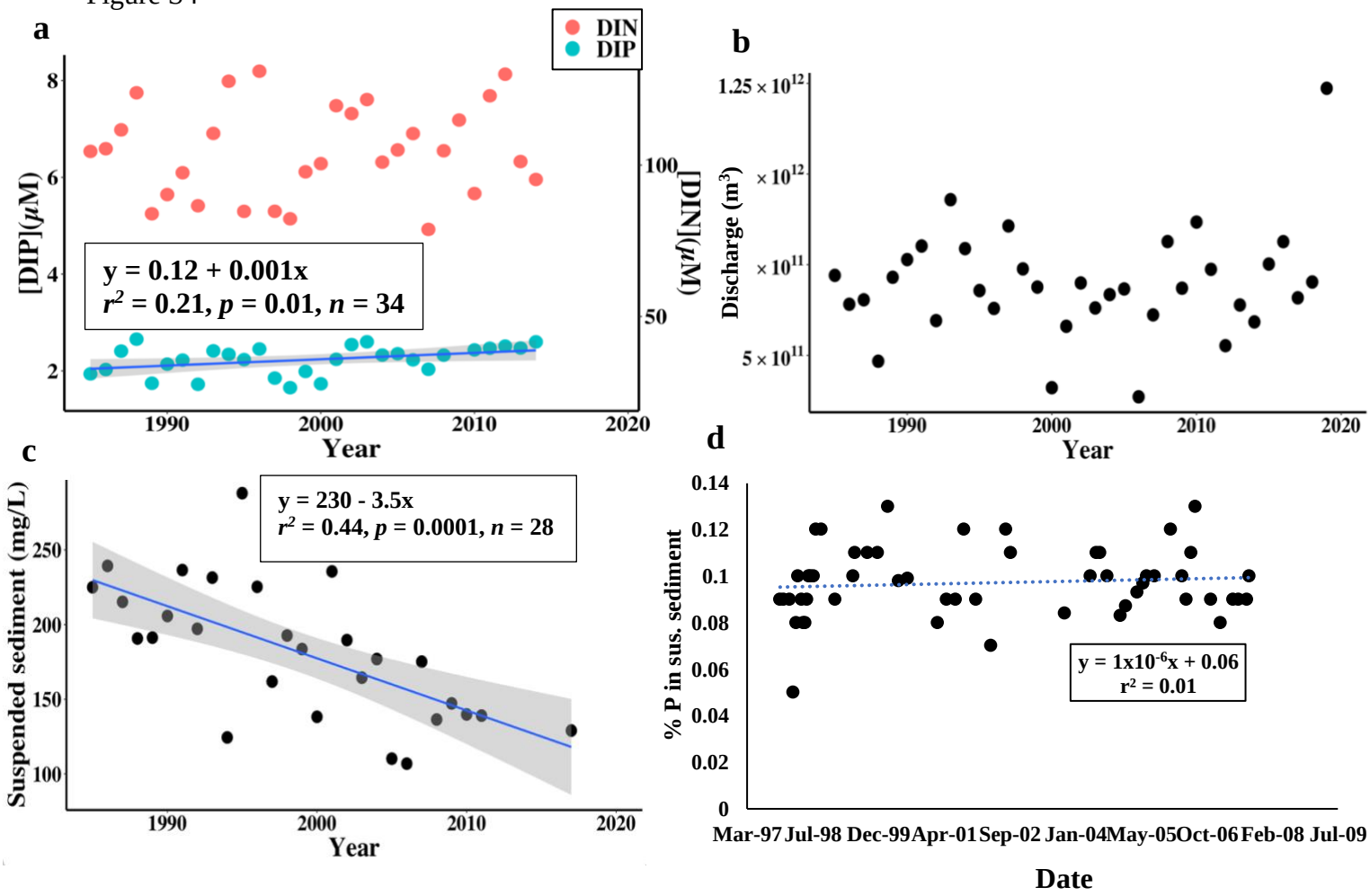

Fig. S4 Annual mean MAR (a) DIN (pink) and DIP (teal) concentrations at St. Francisville, LA, (b) discharge into the NGoM, (c) suspended sediment concentrations at St. Francisville, LA from 1985 to 2019 (see Figure 2 for annual mean nutrient loading into the NGoM 1985–2019), and (d) percentage P in MAR suspended sediment (digested) 1997 to 2009 . Gray shading represents the 95% confidence interval for the statistically significant regression lines. Non-significant regressions are not shown. Based on USGS data (Lee, 2022)

Figure S5

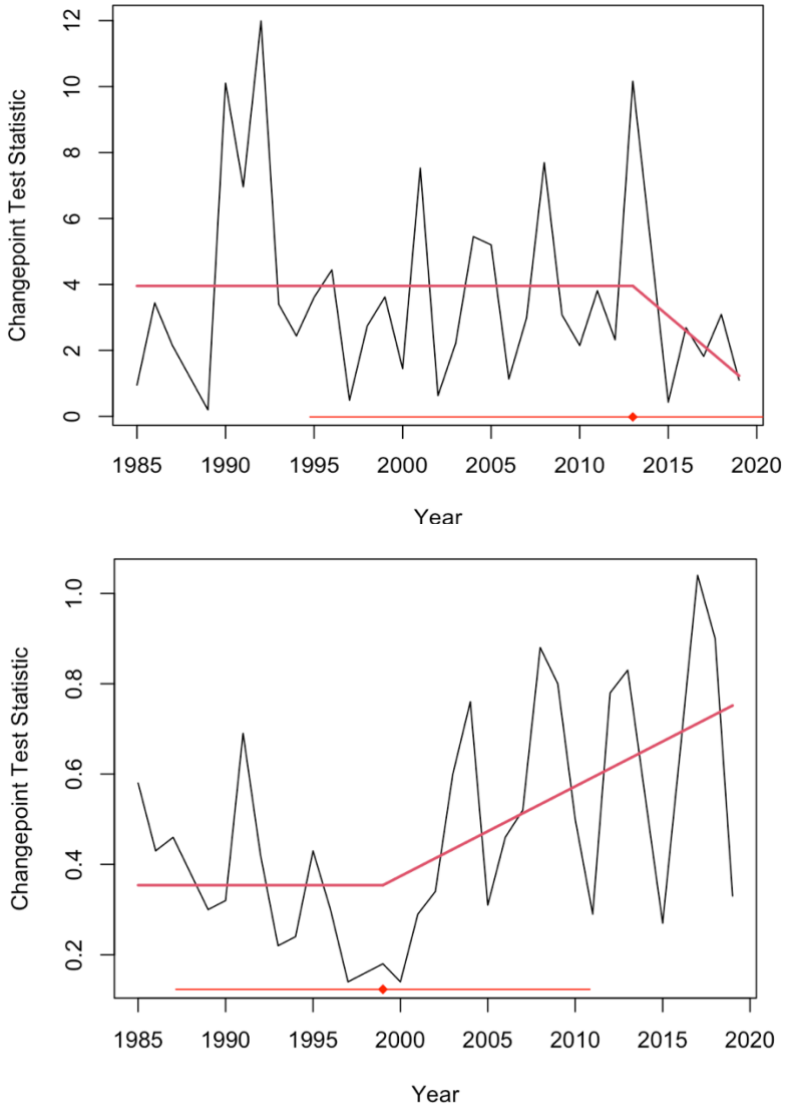

Fig. S5 Changepoint test statistics for NGoM (a.) annual mean DIN over time and (b.) annual mean DIP over time 1985–2019 (excluding 1988 and 2014); A linear regression model with segmented relationships were estimated using the *segmented()* R package for annual mean DIN over time and mean DIP over time to estimate a new regression model for broken-line relationships where the linear relationship changes. The DIN breakpoint is at 2013, and the DIP breakpoint is at 1999, though neither changepoint is significant. The red line above the x axis represents the error bars for the changepoint time statistics

Figure S6

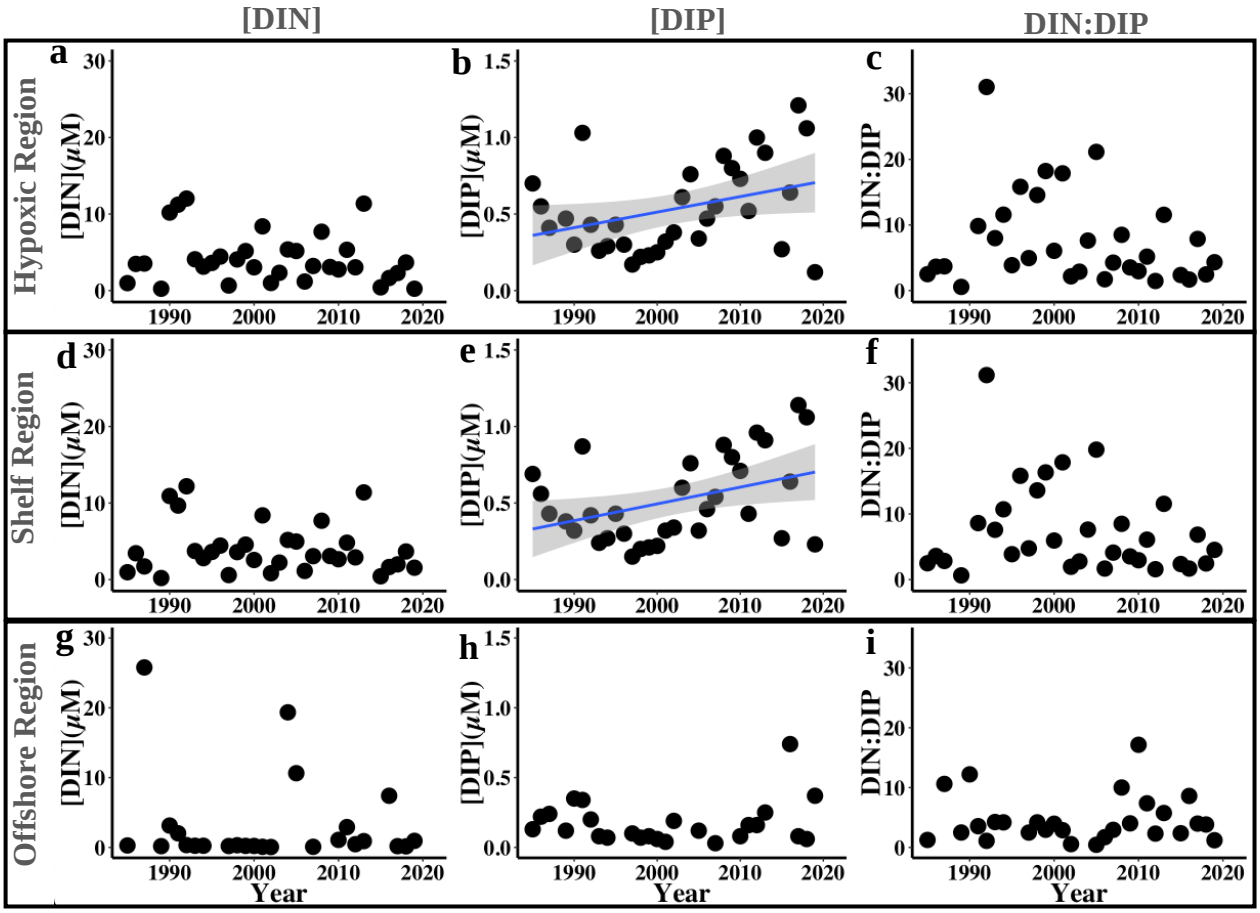

Fig. S6 Annual mean nutrient concentrations (DIN, DIP, and DIN:DIP) for each regional subset of the NGoM 1985–2019 (excluding 1988 and 2014); (a - c) hypoxic, (d - f) shelf, and (g - i) offshore region. Entire dataset annual mean nutrient concentrations (without regional subsets) are shown in Figure 3. Corresponding linear regression equations, r^2, p, and n values are listed in Table S2

Figure S7

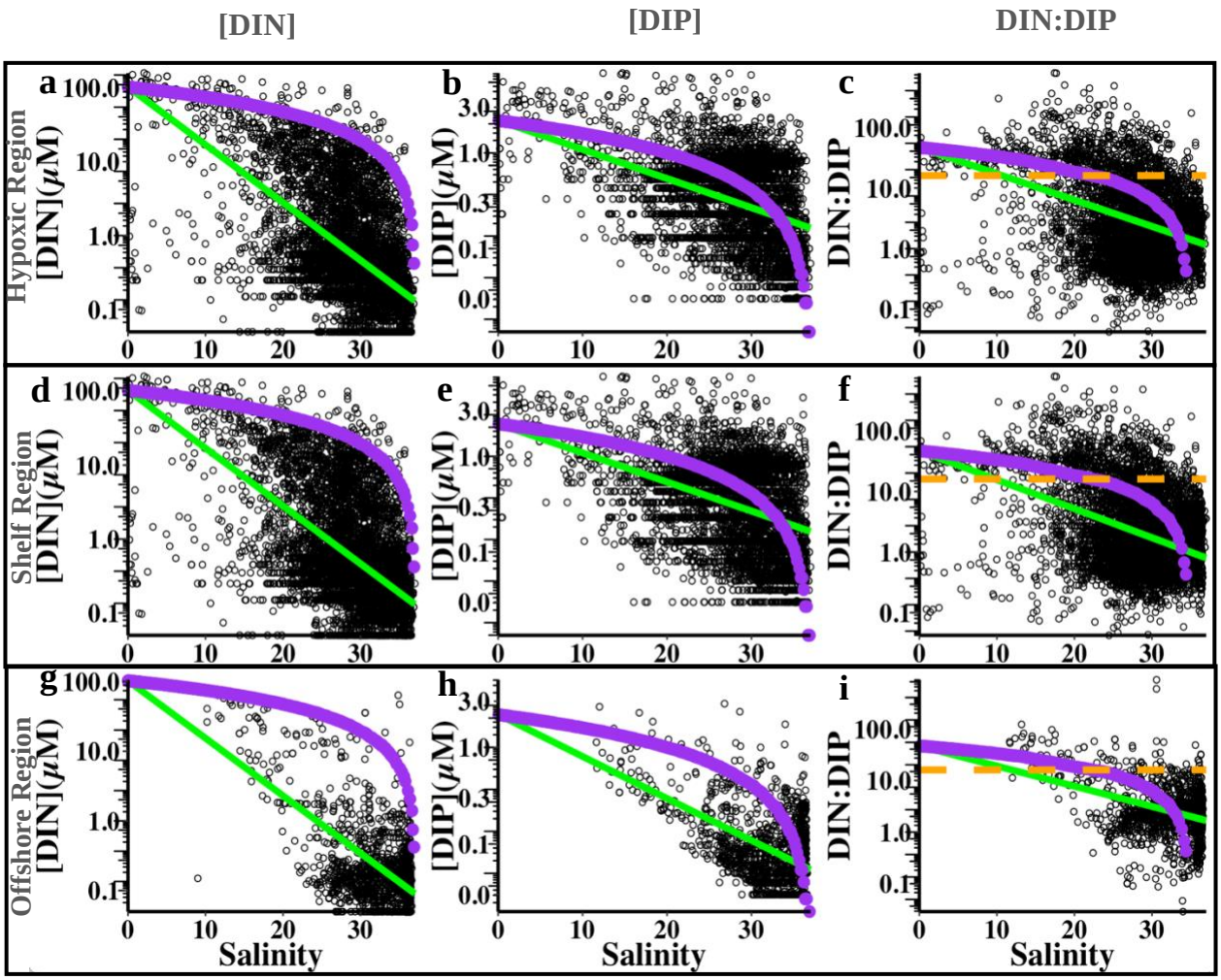

Fig. S7 NGoM surface nutrients vs. salinity by regional subset 1985–2019 (excluding 1988 and 2014): (a) hypoxic [DIN]; (b) hypoxic [DIP]; (c) hypoxic DIN:DIP; (d) shelf [DIN]; (e); shelf [DIP]; (f) shelf DIN:DIP; (g) offshore [DIN]; (h) offshore [DIP]; (i) offshore DIN:DIP – NGoM nutrient concentrations vs. salinity for all regions combined are shown in Figure 4. Black circles represent surface nutrient data, note the log scale of y-axes. The green lines represent linear regressions to ln-transformed data, with the corresponding equations, r^2, p, and n values listed in Table S7. The conservative mixing functions are shown in purple. In the DIN:DIP graphs (c, f, i), the orange dashed line represents the Redfield ratio of DIN:DIP = 16

Figure S8

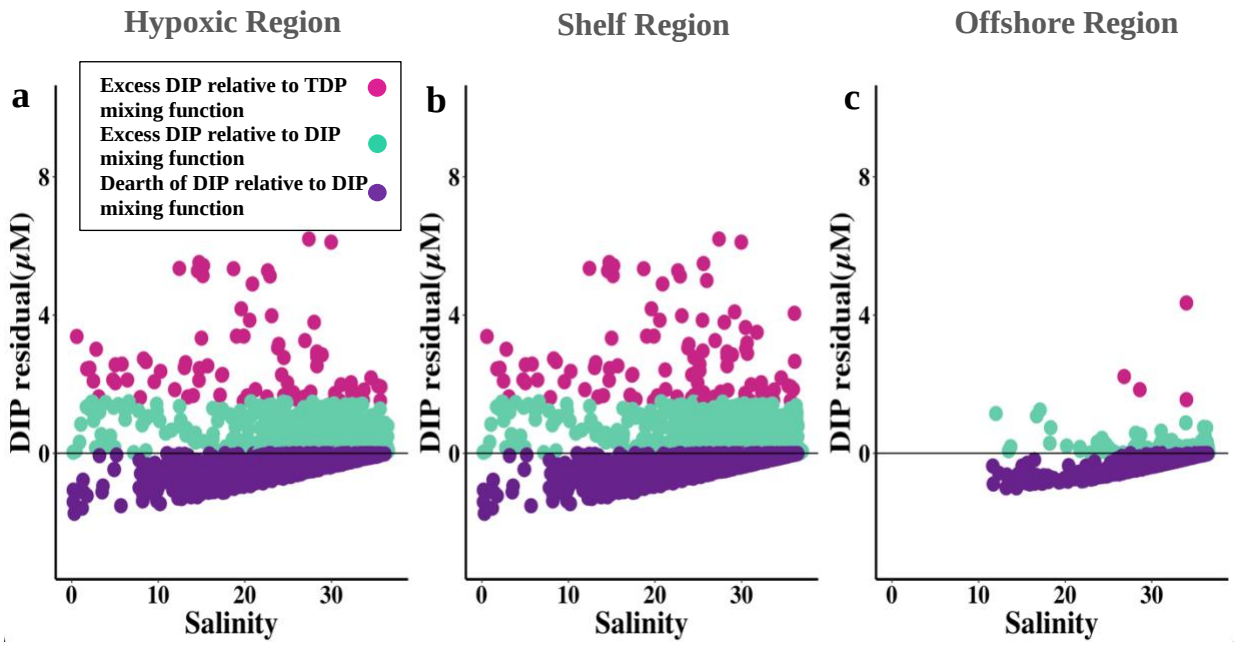

Fig. S8 Residuals of NGoM DIP concentrations (1985-2019) relative to the conservative mixing function connecting MAR DIP and TDP to the offshore endmember, data separated into (a) hypoxic; (b) shelf; and (c) offshore regions. Each point equates to an individual sample and shows the DIP residual relative to the MAR DIP mixing function (y = -0.059x + 2.2). Positive residuals (teal and pink) indicate that the actual values were higher than predicted, and negative residuals (purple) signify that the actual values were lower than predicted by the MAR DIP mixing function. Pink values are positive relative to both the MAR DIP mixing function and would also be positive relative to the MAR TDP mixing function (y = -0.089x + 3.3). Teal values are positive relative to the MAR DIP mixing function, but would be negative relative to the MAR TDP mixing function. Purple values are negative relative to both mixing functions

Figure S9

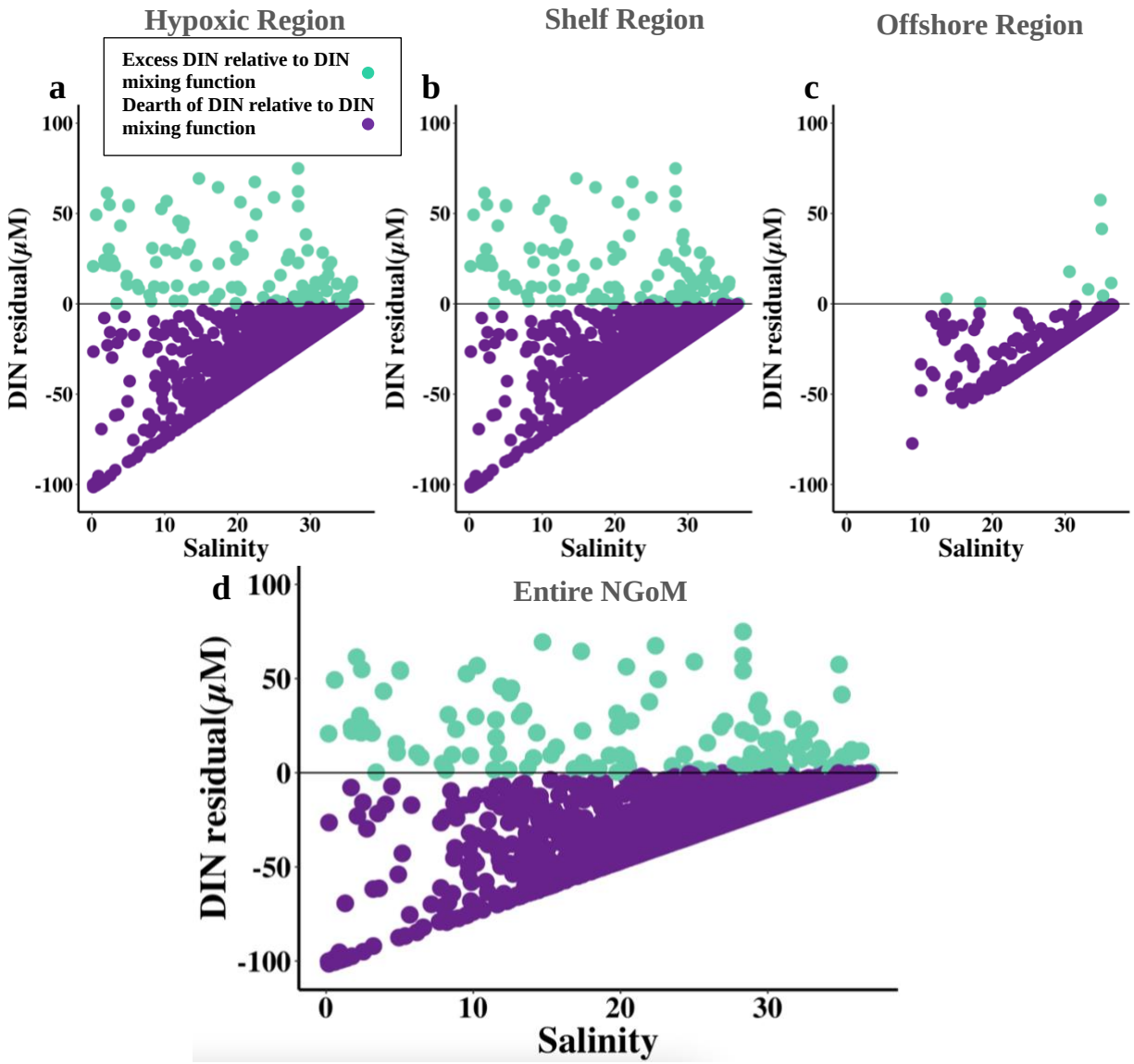

Fig. S9 Residuals of NGoM DIN concentrations (1985-2019) relative to conservative mixing function connecting MAR DIN to the offshore endmember, separated into (a) hypoxic; (b) shelf; (c) offshore regions; and (d) entire NGoM. Each point equates to an individual sample showing the residual relative to the MAR DIN mixing function (y = -2.77x + 102.41). Positive residuals (teal) indicate that actual values were higher than predicted, and negative residuals (purple) signify actual values were lower than predicted by the mixing function